Unified approach to the electronic structure of strained Si/Ge superlattices

C. Tserbak, H. M. Polatoglou, and G. Theodorou
Physics Department, Aristotle University of Thessaloniki, Thessaloniki, GR-54006, Greece
(Received 5 August 1992)

A tight-binding model in the three-center representation, with an orthogonal sp^3 set of orbitals and interactions up to third neighbor, is introduced. This model gives a good description of bulk Si and Ge and reproduces known results for their band structures, including the lowest conduction band, their density of states, effective masses, deformation potentials, and dielectric function. Also, this is an efficient model as far as computer time is concerned; therefore, it is most appropriate for application to superlattices (SL's). In particular, it is used to study the electronic properties of some strained Si/Ge superlattices. Their band structure, confinement of superlattice states, transition probabilities, effective masses, and spin splittings were investigated and the influence of the strain and superlattice periodicity was studied. It was found that under specific conditions of growth, some SL's can be direct-gap materials. Finally, the comparison with experimental results shows that the present model is a realistic one and can be used to describe the electronic properties of the strained Si/Ge SL's and clarify many of the points that are under debate.

I. INTRODUCTION

Recent developments in advanced epitaxial techniques (molecular-beam epitaxy, metal-organic vapor deposition, etc.), have made superlattices (SL's) one of the most promising research fields in semiconductor physics. Among these structures, the coherently grown lattice-mismatched $(Si)_n/(Ge)_m$ superlattices have been the object of considerable interest, since they provide the possibility of designing structures that exhibit desired electronic and optical properties.[1-3] This is possible because these properties can be modified by strain effects, zone folding of the bands, and quantum confinement effects. One of the exciting prospects for these SL's is that of engineering a new direct-gap material from the two constituent materials (Si and Ge), which are indirect semiconductors. The first theoretical work on this subject was carried out by Gnutzmann and Clausecker.[4] The technological importance lies in the expectation that the direct-gap Si/Ge SL's may be used as components in integrated optoelectronic devices, in conjunction with the already well-established and highly advanced silicon technology.

Up to now, a lot of experimental and theoretical works have been reported for the Si/Ge SL's. Most of the experimental work consists of electroreflectance, photoreflectance, piezoreflectance, and photoluminescence measurements.[5-10] Very recently, dielectric function and absorption measurements have also been reported.[11-14] The first samples that have been experimentally investigated were finite SL's grown on Si or Ge. Because of the critical thickness limit of the SL's grown on pure Si or Ge, the idea of strain-symmetrized SL's have been suggested by Kasper *et al.*[15] Special interest has been devoted to structures with $n+m=10$, since theoretical predictions and experimental evidence are in support of the idea that these SL's are direct-gap materials.[9,11,12,16-18] Because of the relative difference in the electronic structure of the constituent materials, the most appropriate theoretical methods for SL band-structure calculations are the microscopic ones. Such methods are the *ab initio* and empirical pseudopotential method, the LMTO (linear-muffin-tin-orbitals) method, the empirical tight-binding method, etc. Indeed many theoretical articles based on previous methods have been published for a variety of Si/Ge SL's.[18-30] From these studies, it seems that the least computationally involved and simplest method is the empirical tight-binding one. It is the aim of the present paper to show that electronic and optical properties of Si/Ge SL's can be reliably calculated with this method.

In the case of Si/Ge strained SL's, the electronic structure of the constituent elements has been extensively studied. It would then be a good test for our model to describe all this knowledge in connection with it in an effective and economical way. For the interpretation of the experimental data, theoretical results concerning the lower conduction and upper valence bands, effective masses, deformation potentials, transition probabilities, and the dielectric function are needed. Many tight-binding schemes have been introduced in the past in order to obtain this information. Up to now, not a single one exists that has been demonstrated to correctly reproduce all the previously mentioned experimental data. The simplest tight-binding approach is to use an orthogonal sp^3 basis set with nearest-neighbor interactions.[31] It is then possible to obtain a quite accurate description of the valence bands but not the conduction ones. Since the conduction bands are important in many phenomena, much effort has been spent on their accurate description. In this spirit, Pandey and Phillips[32] have introduced some second-neighbor interactions. Now the valence bands are accurate but the conduction bands are still not of the same quality. An advance in this problem has been made by Mattheiss and Patel,[33] who have proposed a nonorthogonal tight-binding basis set within the two-center approximation and interactions up to third neigh-

bors. This amounts to a total of 26 nonequivalent interaction parameters. Thus a very good description of the valence and the lowest conduction bands has been achieved. The nonorthogonality of the basis set makes the calculation quite complicated. To avoid these computational difficulties, a very interesting idea has been introduced by Vogl, Hjalmarson, and Dow.[34] These authors have introduced one additional orbital to the minimal sp^3 basis set. This new orbital has been termed s^* and its purpose is to take into account, in an effective way, the d excited atomic states not included in the minimal basis sets. Within this basis set a good description of the lowest conduction bands has been obtained in the Λ and Δ directions of the Brillouin zone (BZ), while the Σ direction, which is important for optical properties, is not well described. In all the above calculations the two-center approximation to the interatomic potential matrix elements has been used. On the other hand, it is more advantageous to use the full three-center representation at the cost of a slightly larger parameter set. Papaconstantopoulos[35] has determined sets of interaction parameters for 53 elements, both two center and three center and with orthogonal and nonorthogonal basis sets. The best description, as expected, is the one with a nonorthogonal basis set and three-center integrals, but it is computationally the most time consuming.

In the previous models, the interaction parameters have been determined for the equilibrium atomic spacing, and no prescription was given as to how these interaction parameters change with the lattice constant or strain. This is a very important issue, since in the Si/Ge SL's the materials are under strain. Brey and Tejedor[26] have carefully adjusted the Vogl, Hjalmarson, and Dow[34] parameters and determined, by comparison to *ab initio* calculations, how the parameters change with a change in the lattice constant. In this way they were the first to determine the electronic structure of the $(Si)_4(Ge)_4$ and $(Si)_6(Ge)_6$ superlattices. An improvement to this approach was the work of Rucker, Enderlein, and Bechstedt.[25] These authors have used three-center integrals and local-field terms to describe the effect of strain on the on-site matrix elements. A very good description of the valence bands and the lowest conduction band has been achieved both in equilibrium and in the presence of strains. As far as the determination of the dielectric function is concerned, there were some unsuccessful attempts.[36,37] It is not clear whether this discrepancy is due to inadequate bands or transition matrix elements, as these quantities together determine the dielectric function.

In our model, we use an sp^3 set of orbitals for each atom and interactions up to third-order neighbors. The orbitals between atoms are assumed to be orthogonal and the three-center representation is used. In addition, the spin-orbit interaction is taken into account. In order to test the validity of our model, we apply it to bulk Si and Ge. In this way we calculate the interaction parameters of the model for these materials. Using these parameters, we obtain the band structure, transition probability, effective masses, and optical properties for bulk Si and Ge. Furthermore, we describe how to obtain, through a scaling relation, the interaction parameters for the strained materials. In this way, we are able to calculate the deformation potentials of these materials. Having the interaction parameters for bulk Si and Ge, we can then apply the same model to strained Si/Ge SL's. Their band structure, confinement effects, effective masses, and spin splittings are studied. In addition, we determine the influence of valence-band offset (VBO) on the band structure, and compare the present theoretical results to experiment.

There is much experimental data on various Si/Ge SL's, mainly from photoluminescence, electroreflectance, absorptance, and piezoreflectance experiments. Their interpretation is difficult, since these are complicated spectra. In addition, there is recent evidence that some of these spectra may contain artifact structures not originating from the SL. With this in mind, we will attempt a comparison of the first allowed transitions, calculated with the use of the present model, to the experimental ones. The motivation is to see if there is some consistent agreement and discuss the cases where this is not true.

The paper is organized as follows: in Sec. II, the description of bulk Si and Ge in terms of our model is presented. Their band structure, density of states, optical properties, and deformation potentials are analyzed. Section III deals with the strained Si/Ge superlattices. In particular, the band structure of Si/Ge SL's is studied, and the influence of periodicity $(n+m)$, composition (n/m), strain, and valence-band offset is investigated. Also, effective masses and spin splittings are calculated and discussed. A comparison with experimental results is also given. Finally, in Sec. IV, we give our conclusions.

II. BULK MATERIALS

A. Band structure

The band structures of bulk Si and Ge have been calculated with the use of several methods, the results being in general agreement. We have described these materials with our model and adjusted the values of the interaction parameters so as to obtain agreement with the results of previous methods. The starting values for the interaction parameters were taken to be the corresponding ones given by Papaconstantopoulos.[35] During the adjustment procedure, attention was paid to obtain a good description of the upper valence and lowest conduction bands, which mainly determine the optical properties. As an input, the bands calculated by Chelikowsky and Cohen,[38] using nonlocal empirical pseudopotentials (EP's) have been used. The resulting set of interaction parameters is given in Table I, in the notation of Slater and Koster. In Figs. 1 and 2, the resulting electronic structures of Si and Ge, respectively, are presented. The spin-orbit interaction is included. In Table II, comparison is made, for some key energies, between the tight-binding results and those of nonlocal empirical pseudopotentials.

For the case of Si our results compare well to those of EP calculations. The main features of the bands are reproduced quite accurately. More specifically, the highest valence and lowest conduction bands run parallel

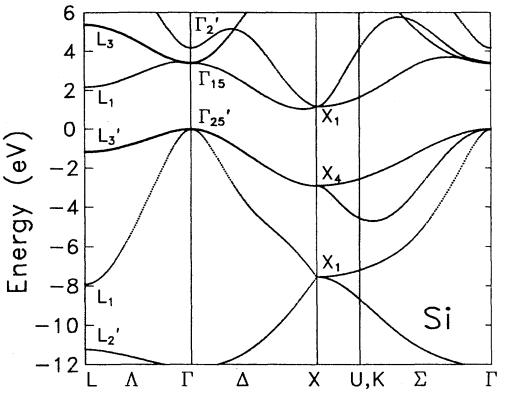

FIG. 1. The energy-band structure of Si, calculated with the present tight-binding model. The top of the valence bands is set at zero energy.

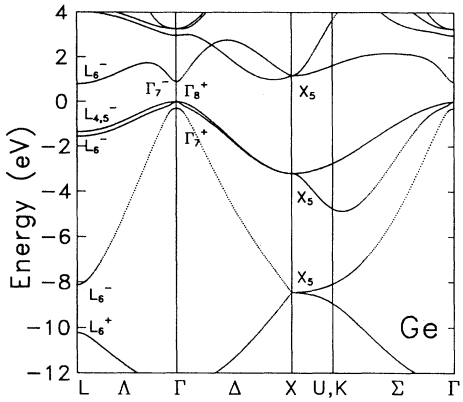

FIG. 2. The energy-band structure of Ge, calculated with the present tight-binding model. The top of the valence bands is set at zero energy.

along the Λ direction, a very important feature for the determination of the E_1 structure in the dielectric function. In addition, the bands are well described around the X point and more specifically along the Δ and Σ directions. Concerning the Σ direction, only a few tight-binding models have achieved such a good description. The distance between the conduction-band minimum Δ_1^c and the Γ point is equal to $0.89(2\pi/a)$, where a is the lattice constant. The lowest direct and indirect gaps are given in Table III, and are in good agreement with the experiment.[31,39–41]

For the case of Ge, our results are also in good agreement with those of EP calculations. A comparison of the present band energies to those calculated with the nonlocal empirical pseudopotential method, Table II, shows that the agreement is very good. The same is true for the values of the fundamental and direct gap, in comparison with the experimental data as given in Table III.

TABLE I. Interaction parameters (in eV) for our tight-binding model which resulted from fitting to the nonlocal empirical pseudopotential band structure. (The notation is that of Slater-Koster.)

	Silicon	Germanium
$E_{ss}(0,0,0)$	−6.3193	−7.2114
$E_{pp}(0,0,0)$	2.2494	1.6376
$E_{ss}(0.25,0.25,0.25)$	−1.8376	−1.3711
$E_{sx}(0.25,0.25,0.25)$	1.0087	0.9127
$E_{xx}(0.25,0.25,0.25)$	0.3209	0.2979
$E_{xy}(0.25,0.25,0.25)$	1.4889	1.2935
$E_{ss}(0.5,0.5,0.0)$	0.1940	0.1150
$E_{sx}(0.0,0.5,0.5)$	−0.0395	0.0250
$E_{sx}(0.5,0.5,0.0)$	−0.1840	−0.0724
$E_{xx}(0.5,0.5,0.0)$	0.0626	0.0710
$E_{xx}(0.0,0.5,0.5)$	−0.2646	−0.1683
$E_{xy}(0.5,0.5,0.0)$	−0.0378	−0.0748
$E_{xy}(0.0,0.5,0.5)$	−0.0829	−0.1298
$E_{ss}(0.75,0.25,0.25)$	−0.0674	−0.1036
$E_{sx}(0.75,0.25,0.25)$	0.2717	0.1710
$E_{sx}(0.25,0.25,0.75)$	−0.1262	−0.0432
$E_{xx}(0.75,0.25,0.25)$	0.0869	0.1287
$E_{xx}(0.25,0.25,0.75)$	0.0094	−0.0092
$E_{xy}(0.75,0.25,0.25)$	0.0152	−0.0076
$E_{xy}(0.25,0.25,0.75)$	0.0952	0.0659
$\lambda_{s.o.}$	0.0150	0.1000

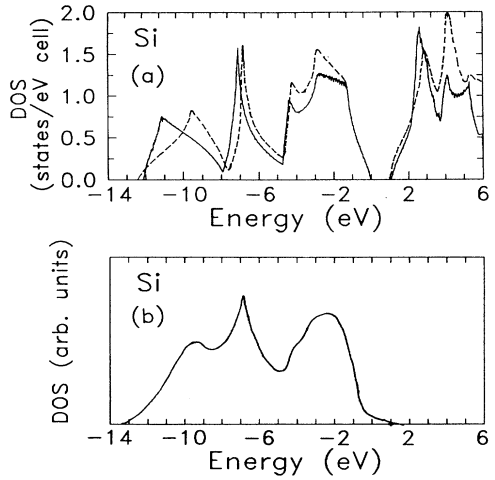

FIG. 3. The density of states of Si. (a) Comparison between the present tight-binding model (solid line) and the nonlocal empirical pseudopotential method (dashed line), and (b) experimental results of Ref. 42.

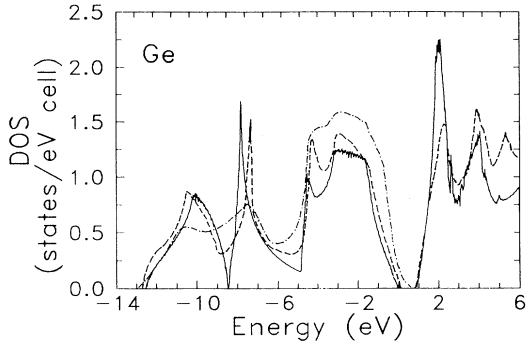

FIG. 4. The density of states of Ge: The experimental results of Ref. 43 (dashed-dotted line), the present tight-binding results (solid line), and the nonlocal empirical pseudopotential results (dashed line) are presented.

B. Density of states

As another check for the quality of the parameters yielded by our model, we have calculated the density of states (DOS) for Si and Ge, a property that provides a good test since it depends not only on the band energies but also on their gradient with respect to the wave vector (group velocity). The calculations were performed with the tetrahedral method by dividing the fundamental unit cell of the reciprocal lattice into 725×10^3 tetrahedra. This is a large number to guarantee that there will be no significant errors in the calculation. The resulted DOS for Si is presented in Fig. 3(a), along with one from a nonlocal empirical pseudopotential method. The two

TABLE II. Eigenvalues (in eV) at Γ, X, L, and K points. A comparison is made to the corresponding eigenvalues of nonlocal empirical pseudopotentials.

	TB	*EP*		*TB*	*EP*
			Silicon		
Γ_1^v	−12.13	−12.36	$L_{2'}^v$	−11.21	−9.55
$\Gamma_{25'}^v$	0.00	0.00	L_1^v	−7.90	−6.96
Γ_{15}^c	3.41	3.43	$L_{3'}^v$	−1.16	−1.23
$\Gamma_{2'}^c$	4.18	4.10	L_1^c	2.17	2.26
			L_3^c	5.39	4.34
X_1^v	−7.54	−7.69	K^v	−8.18	−8.69
X_4^v	−2.89	2.86	K^v	−7.25	−7.18
X_1^c	1.16	1.18	K^v	−4.28	−4.56
			K^v	−2.50	−2.54
			K^c	1.58	1.66
			Germanium		
Γ_6^v	−12.56	−12.66	L_6^v	−10.22	−10.39
Γ_7^v	−0.30	−0.30	L_6^v	−8.13	−7.61
Γ_8^v	0.00	0.00	L_6^v	−1.56	−1.63
Γ_7^c	0.90	0.90	$L_{45'}^v$	−1.36	−1.43
Γ_6^c	2.97	3.01	L_6^c	0.79	0.76
Γ_8^c	3.27	3.22	L_6^c	4.04	4.16
X_5^v	−8.45	−8.65			
X_5^v	−3.19	3.29			
X_5^c	1.17	1.16			

TABLE III. Calculated values for the gaps (in eV) compared to experiment.

	Theory	Experiment
	Silicon	
$E_0'(\Gamma_{25'}^v-\Gamma_{15}^c)$	3.41	3.40[a], 3.38[b]
$E_g^i(\Gamma_{25'}^v-\Delta_1^c)$	1.05	1.13[c]
	Germanium	
$E_0(\Gamma_8^v-\Gamma_7^c)$	0.90	0.90[d]
$E_g^i(\Gamma_8^v-L_6^c)$	0.76	0.76[c]

[a]Zucca and Shen (Ref. 39).
[b]Jellison and Modine (Ref. 40).
[c]Harrison (Ref. 31).
[d]Zwerdling (Ref. 41).

curves agree well in the region of valence bands and quite well for the conduction bands up to 4 eV. In Fig. 3 (b), the experimental data are presented. In Fig. 4, the calculated DOS for Ge, using the present parametrization, is presented along with the pseudopotential results and the experimental data. The comparison is better than that of Si.[42,43]

C. Effective masses

The electron and hole effective masses is another set of important parameters which influence many phenomena such as transport of electrons and holes, excitonic states, etc. The calculated hole effective masses at the Γ point, for the [111] and [100] directions, are given in Table IV, along with the experimental data. The heavy-hole masses are the most anisotropic ones, while the spin-split holes are almost isotropic, and for that reason only one value is presented. In general, the agreement with the experimental values is good. The largest deviation occurs for the heavy holes of Ge along the [111] direction. In Table V, the calculated electronic effective masses at Γ and at the minimum of the conduction band are presented and compared with the experimental ones. From this table, it is evident that m_T^* agrees well for Si but deviates greatly for Ge. Also, m_L^* deviates in both cases by as much as 40%. The theoretical values are in all cases lower than the experimental ones. This underestimation is quite understandable, since in these calculations phenomena such as the electron-phonon interaction were not included. Such effects have been discussed by Beni and Rice,[49] and it was found that they tend to increase the effective mass. Therefore, the discrepancy is not as serious as the numbers indicate.

D. Optical properties

Many optical properties, such as the dielectric function, the reflectivity, absorptance, etc., are related to the band structure of crystalline solids. Most of them can be derived from the dielectric function $\varepsilon(\omega)=\varepsilon_1(\omega)+i\varepsilon_2(\omega)$ by appropriate relations. In addition, the dielectric function can be measured directly and reliably by spectroscopic ellipsometry. Therefore, it is worth calculating this property for Si and Ge. The imaginary part of the dielectric function is calculated in the random-phase approximation with the momentum matrix elements calculated using the relation

$$P=\frac{m}{\hbar}\frac{dH(k)}{dk}\ . \tag{1}$$

The real part ε_1 of the dielectric function is calculated by a Kramers-Kroning relation, with the contribution from energies larger than 10 eV taken into account by the tail formula $\beta\omega/(\omega^2+\gamma^2)^2$,[50] where parameters β and γ are determined by the continuity condition.

Figure 5(a) shows the calculated ε_2 of Si, as a function of the photon energy, along with the experimental data. Notice that the onset of ε_2 occurs at 3.33 eV, while for higher energies it rises very steeply and reaches a value around 25, at an energy of only 0.3 eV above the onset. This behavior is due to the parallel valence and conduction bands along the Λ direction. The contribution of the different interband transitions to ε_2 is also calculated (Fig. 6). It is obvious that the main contributions to E_1 and E_2 structures come from transitions between the highest valence and the lowest conduction band ($4\rightarrow5$); the numbering of the bands starts from the lowest valence band. The Van-Hove singularity associated to the E_1 structure, occurring at 3.55 eV, is due to transitions along the Λ direction. Two Van-Hove singularities are associated to the E_2 structure and appear at energies of 4.09 and 4.5 eV. The first one results from transitions close to point X, and the second one from the Σ direction.

TABLE IV. Calculated hole effective masses of Si and Ge in units of the free-electron mass, m_0.

	$m_{\rm lh}^*[100]$	$m_{\rm lh}^*[111]$	$m_{\rm hh}^*[100]$	$m_{\rm hh}^*[111]$	$m_{\rm s.o.}^*$
			Si		
Expt.	0.153[a]		0.537[a]		0.234[a]
Theory	0.147	0.133	0.533	0.854	0.234
			Ge		
Expt.	0.044[b]	0.043[b]	0.284[b]	0.376[b]	0.095[c]
Theory	0.060	0.056	0.381	0.728	0.137

[a]Barber (Ref. 44).
[b]Dexter, Zeiger, and Lax (Ref. 45).
[c]Aggarwal (Ref. 46).

TABLE V. Calculated electron effective masses of Si and Ge in units of m_0 at Γ and the minimum of the conduction band.

Si	m_c^*	$m_L^*(\Delta)$	$m_T^*(\Delta)$
Experiment		0.916[a]	0.191[a]
Theory	0.528	0.568	0.173
Ge	m_c^*	$m_L^*(L)$	$m_T^*(L)$
Experiment	0.038[b]	1.570[c]	0.081[c]
Theory	0.052	0.990	0.129

[a]Hensel, Hasegawa, and Wakayama (Ref. 47).
[b]Aggarwal (Ref. 46).
[c]Fink and Braunstein (Ref. 48).

The bulk of the transitions that contribute to the E_2 structure comes from a large volume of the BZ around the point (0.6,0.6,0.2) ($2\pi/a$). The calculated real part of the dielectric function, ε_1, is presented in Fig. 5(b), along with the experimental spectra. One can observe that the results of our calculations for ε_2 and ε_1 are quite close to the experimental ones, with the exception of the region near the E_1 structure. This discrepancy is due to excitonic effects not included in our calculations. The value of ε_1 at zero energy, related to a sum rule for transition probabilities, is found equal to 10.5, while the experimental value is 11.7.[52] The 10% deviation may be attributed to many-body phenomena.

The dielectric function of Ge is presented in Fig. 7 and compared with the experimental data of Vina, Logothetidis, and Cardona.[53] The onset of ε_2 appears at 0.9 eV, which corresponds to the lowest direct gap at the center of the BZ. In contrast to Si, here we have well-resolved structures resulting from spin-split-off bands, because of the larger spin-orbit interaction. The E_1 structure is well separated from the E_2 by as much as 2 eV. The contribution of the different interband transitions to ε_2 is given in Fig. 8, from where it can be seen that the main contribution comes from the transitions $4\rightarrow5$, with a significant contribution from the interband transitions $3\rightarrow5$. The steep rise of ε_2 at energies around 2 eV is due to the parallel bands along the Λ direction. The energies of the Van-Hove singularities that contribute to E_1 and $E_1+\Delta_1$ structures are 2.24 and 2.44 eV, respectively. The main peak in ε_2, occurring at 4.4 eV, results from an extended region of the BZ around the point (0.75,0.2,0.2) ($2\pi/a$), and a small region around point K. The so-called E_0' structure occurs at 3.4 eV. There are also two structures which have been denoted with E_1' and which occur at energies of 5.4 and 5.8 eV. The interband transitions responsible for these structures are the $3\rightarrow6$ and $4\rightarrow6$, around the L point. Our results show, in addition, a small structure at 4.82 eV, which has no counterpart in the experimental spectra. This structure is due to transitions around the X point. The good description of the dielectric function is a justification for the validity of formula (1), used for the calculation of momentum matrix elements.

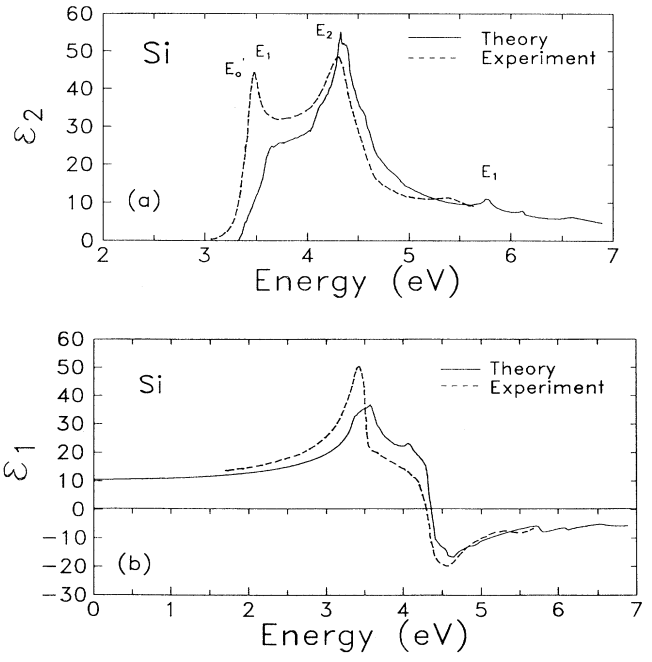

FIG. 5. The dielectric function of Si. (a) Imaginary part $\varepsilon_2(\omega)$ and (b) real part $\varepsilon_1(\omega)$. The experimental curves are from Ref. 51. The different structures are indicated in (a).

E. Deformation potentials

The influence of strain results in a change of the atomic positions in the crystal. The determination of the new positions is a difficult problem. For relatively small strain, the problem can be approached by the theory of elasticity. This condition holds to a good degree in the case of strained Si/Ge superlattices. Therefore, before going on to the SL case, we need to know the properties of strained Si and Ge along the [001] direction.

In the tight-binding method, the matrix elements of the Hamiltonian are sums of products of three-center integrals with phase factors.[54] For the matrix elements between orbitals located on nearest-neighbor atoms, the three-center integrals can be expressed as products of two-center integrals with directional cosines. These two

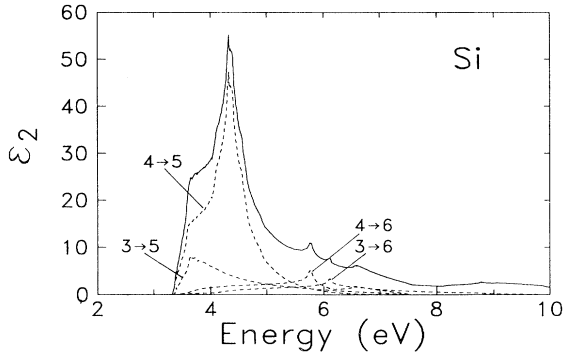

FIG. 6. The decomposition of $\varepsilon_2(\omega)$ for Si into different interband contributions. The most significant parts are shown.

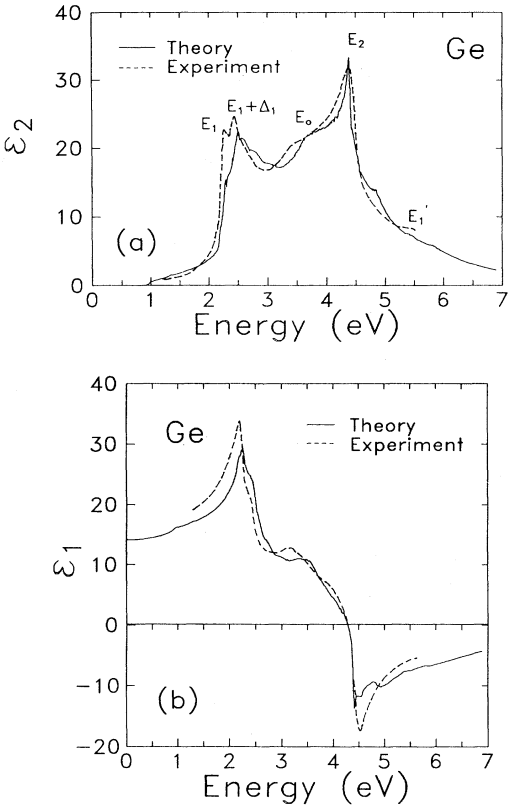

FIG. 7. The dielectric function of Ge. (a) Imaginary part $\varepsilon_2(\omega)$ and (b) real part $\varepsilon_1(\omega)$. The experimental curves are from Ref. 53. The different structures are indicated in (a).

center integrals are independent of the directional cosines. In addition, we assume that the more distant three-center integrals are independent of directional changes induced by a small strain. For these two-center integrals, as well as the more distant three-center integrals, it has been deduced from several calculations[31,55,56] that a power-law scaling of the form

$$H_{\alpha\beta}=H^0_{\alpha\beta}(d_0/d)^v \tag{2}$$

is appropriate. In addition, the uniaxial strain lifts the degeneracy between the p_z and p_x,p_y orbitals. In the linear approximation, the on-site p-orbital integrals are equal to

$$E_p^{x,y}=E_p+b_p(\varepsilon_\parallel-\varepsilon_\perp),\quad E_p^z=E_p-2b_p(\varepsilon_\parallel-\varepsilon_\perp)\ , \tag{3}$$

where $\varepsilon_\parallel$ and $\varepsilon_\perp$ are the strain components parallel and perpendicular to the interface, and b_p is an appropriate uniaxial splitting parameter.

In many cases, the exponent v in Eq. (2) was chosen equal to 2,[31,56] independent of the orbitals involved in the matrix elements, but, as was later shown,[57] a more judicious choice of the exponent results in a better description of the strained system. For this reason we choose to have exponents that depend upon the orbitals. The aim of the present section is to obtain good values for the deformation potentials for Si and Ge by adjusting the exponent of the scaling law, as well as b_p. The strain under consideration has two components, a hydrostatic and a uniaxial one. In addition, the electronic states of interest are those of band maxima and minima at the Γ point, and those of the conduction-band minima in the Δ direction and at the L point. The change in energy of the above states under hydrostatic and uniaxial strain along the [001] direction, in terms of (a) the absolute hydrostatic deformation potentials a^c and a^v for the conduction- and valence-band extrema, respectively, at the Γ point; (b) the absolute deformation potentials $\Xi_d^L+\frac{1}{3}\Xi_u^L$ and $\Xi_d^\Delta+\frac{1}{3}\Xi_u^\Delta$ for the conduction-band extrema at the L point and the Δ direction, respectively; (c) the uniaxial deformation potential b for the top of the valence band; and (d) the uniaxial deformation potential Ξ_u^Δ for the conduction-band minima along the Δ direction, is given by [58]

$$\begin{aligned}
\delta E(V_2)&=-\delta E_h^v-(\tfrac{1}{2})\delta E_{001}\ ,\\
\delta E(V_1)&=-(\tfrac{1}{2})\Delta_0-\delta E_h^v+(\tfrac{1}{4})\delta E_{001}\\
&\quad+\tfrac{1}{2}\sqrt{[\Delta_0^2+\Delta_0\delta E_{001}+(\tfrac{9}{4})(\delta E_{001})^2]}\ ,\\
\delta E(V_3)&=(\tfrac{1}{2})\Delta_0-\delta E_h^v+(\tfrac{1}{4})\delta E_{001}\\
&\quad-\tfrac{1}{2}\sqrt{[\Delta_0^2+\Delta_0\delta E_{001}+(\tfrac{9}{4})(\delta E_{0001})^2]}\ ,\\
\delta E(\Delta_{xy})&=[\Xi_d^\Delta+(\tfrac{1}{3})\Xi_u^\Delta]\,\mathrm{Tr}[\varepsilon]+(\tfrac{1}{3})\Xi_u^\Delta(\varepsilon_\parallel-\varepsilon_\perp)\ ,\\
\delta E(\Delta_z)&=[\Xi_d^\Delta+(\tfrac{1}{3})\Xi_u^\Delta]\,\mathrm{Tr}[\varepsilon]-(\tfrac{2}{3})\Xi_u^\Delta(\varepsilon_\parallel-\varepsilon_\perp)\ ,\\
\delta E(L)&=[\Xi_d^L+(\tfrac{1}{3})\Xi_u^L]\,\mathrm{Tr}[\varepsilon]\ ,
\end{aligned} \tag{4}$$

with $\delta E_h^v=a^v\mathrm{Tr}[\varepsilon]$, $\delta E_{001}=-2b(\varepsilon_\parallel-\varepsilon_\perp)$, Δ_0 the spin-orbit splitting at Γ, and $[\varepsilon]$ the strain tensor.

The values of v resulting from the above-mentioned adjustment for Si and Ge are $v_{ss}=3$ and $v_{pp}=v_{sp}=1.8$. We observe that the values of v for the pp and sp interactions is very close to 2. The calculated values for the deformation potentials are then given in Table VI, along with the experimental ones. Taking into consideration the spread of the experimental values, we conclude that the comparison between theory and experiment is satisfactory. A discrepancy appears (wrong sign) in the value of the deformation potential $\Xi_d^\Delta+\frac{1}{3}\Xi_u^\Delta$ for Si. This discrepancy is

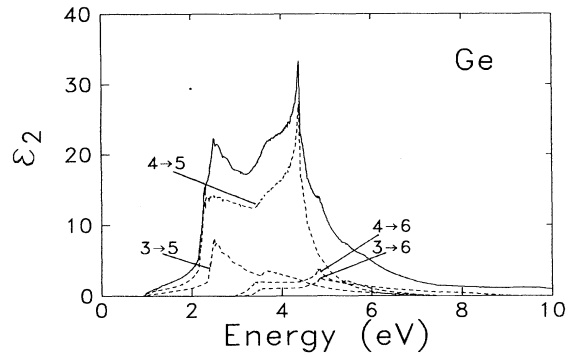

FIG. 8. The decomposition of $\varepsilon_2(\omega)$ for Ge into different interband contributions. The most significant parts are shown.

TABLE VI. Calculated deformation potentials (in eV) compared to experiment.

Deformation potentials	Si TB	Si Expt.	Ge TB	Ge Expt.
a^c-a^v	−11.84		−9.13	−9.2[a], −9.5[b]
$\Xi_d^\Delta+(\frac{1}{3})\Xi_u^\Delta-a_v$	−0.77	1.41[b], 1.5±0.3[c]	−0.9	
$\Xi_d^L+(\frac{1}{3})\Xi_u^L-a_v$	−4.42		−2.64	−2.0±0.5[d], −3.8[e]
b	−2.21	−2.1±0.1[c]	−2.5	−2.8±60.15[f]
Ξ_u^Δ	8.86	8.6±0.4[c]	7.24	

[a]Goni, Syassen, and Cardona (Ref. 61).
[b]Landolt-Börnstein (Ref. 59).
[c]Laude and Pollak (Ref. 60).
[d]Balslev (Ref. 62).
[e]Paul and Warschauer (Ref. 63).
[f]Chandrasekhar and Pollak (Ref. 64).

mainly due to the exclusion of the d orbitals from the basis set. In the tight-binding model of Brey and Tejedor,[26] where the effect of the d orbitals was partially included through the s^* orbital, the latter deformation potential has been correctly described. It should be noted, however, that deviations in this deformation potential are not important for the description of strained Si. This is due to the fact that the position of the conduction-band minima is determined mainly from the uniaxial deformation potential Ξ_u^Δ, whose value is approximately six times larger than that of $\Xi_d^\Delta+(\frac{1}{3})\Xi_u^\Delta$.

Strain in Si and Ge can be produced by growth on a $Si_{1-x}Ge_x$ substrate. The lattice constant of the substrate is well described by the Vegard law, according to which it is a linear function of x. For pseudomorphic growth on this substrate, the lattice constant of the material along the growth plane is defined by the substrate lattice constant, and the perpendicular one by Poisson's ratio. Therefore, the concentration x of Ge in the substrate defines the strain. We have calculated the energies of the valence-band maxima (V_1, V_2, V_3) and the conduction-band minima (Δ_{xy}, Δ_z, and L) as a function of x for strained Si (s-Si) and strained Ge (s-Ge) grown coherently on the surface (001) of the $Si_{1-x}Ge_x$ alloy. The results are presented in Fig. 9. The continuous lines are determined by relations (4), using the experimental values of the deformation potentials. The change in the valence-band energies, as well as the splitting $|E(\Delta_{xy})-E(\Delta_z)|$ for s-Si and s-Ge, are in good agreement with the experimental results. In the case of s-Si, the conduction-band minimum always occurs in the Δ_z direction, while in the case of s-Ge it occurs in the Δ_{xy} direction for $x<0.33$ and at the L point for $x>0.33$.[59–64]

Finally, the band structures of s-Si and s-Ge have been calculated. In Figs. 10 and 11, the results are shown for the band structure of s-Si grown on the Ge(001) substrate and s-Ge grown on Si(001), respectively. For the case of s-Si, the upper valence state has p_z character, while for the case of s-Ge it has p_x, p_y character. For the s-Si, the top two valence bands have, along the Δ_{xy} direction, a splitting of about 0.3 eV, while along Δ_z they are almost degenerate, and along ΓN the splitting is about 0.2 eV. The case of Ge is similar. Notice here a splitting of 0.4 eV along the ΓN direction.

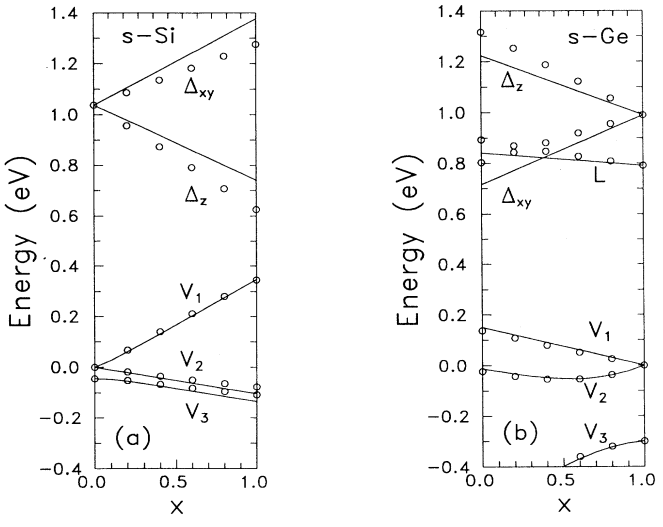

FIG. 9. Energies of the three top valence states at Γ (V_1, V_2, V_3) and the lowest conduction states at Δ_{xy}, Δ_z and L for biaxially distorted (a) Si and (b) Ge, grown on a $Si_{1-x}Ge_x$(001) surface, as a function of x.

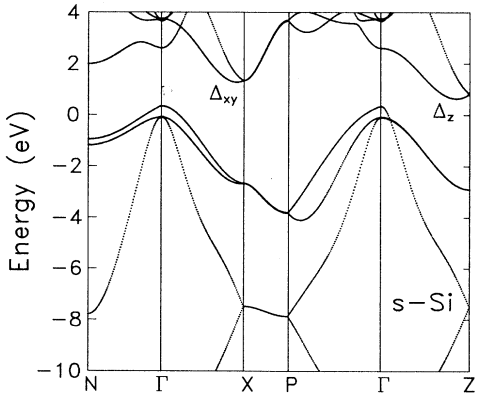

FIG. 10. The band structure of strained Si, coherently grown on a bulk Ge(001) surface.

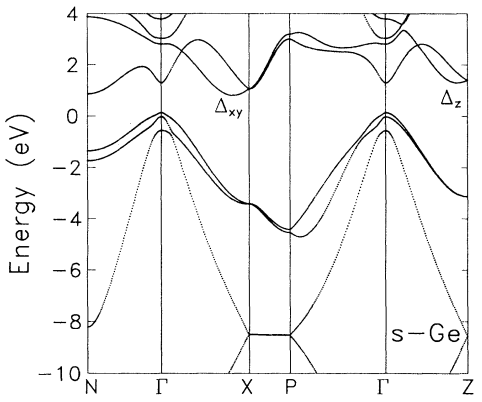

FIG. 11. The band structure of strained Ge, coherently grown on a bulk Si(001) surface.

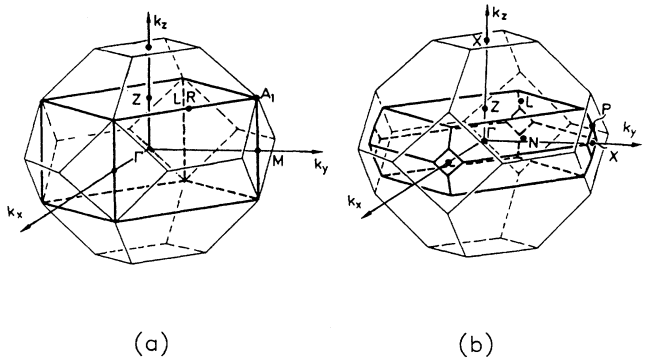

FIG. 12. The Brillouin zone for superlattices with $(n+m)/2$ (a) even and (b) odd.

III. SUPERLATTICES

A. Structure and symmetry

Both Si and Ge crystallize in the diamond structure, but their lattice constants differ by about 4.2%. As a result, the Si/Ge superlattices are under internal stress. This stress produces a distortion of the lattices and creates dislocations for the case of thick layers. For thin layers, the growth can be pseudomorphic (without dislocations), in which case the lateral lattice constant is the same in the Si and Ge layers and equal to that of the substrate and, for growth on the $Si_{1-x}Ge_x$ alloy, is, to a good approximation, given by Vegard's law:

$$a_{\parallel}=(1-x)a_{\mathrm{Si}}+xa_{\mathrm{Ge}} \ . \tag{5}$$

For pseudomorphic growth, the lattice constant along the growth axis is given with good accuracy by Poisson's ratio.[65] The strain in each layer will then be given by

$$\varepsilon_{\parallel}^{i}=\frac{a_{\parallel}}{a_i}-1 \tag{6}$$

and

$$\varepsilon_{\perp}^{i}=\frac{2v_i}{1-v_i}\varepsilon_{\parallel}^{i} \ , \tag{7}$$

where a_i is the lattice constant of the undistorted bulk material and v_i the corresponding Poisson ratio.

According to valence-force-field calculations[66,67] and self-consistent total-energy pseudopotential calculations,[21] the interlayer distance at the interface is fairly close to the mean value of the interlayer distance in the distorted materials.

The crystal symmetry of $(Si)_n/(Ge)_m$ SL's has been studied in detail.[68,69] When both n and m are even, the structure is orthorhombic. If at least one of n or m is odd, then the structure is tetragonal The space groups for each case are given in Table VII, and the superlattice Brillouin zone (SBZ) for $(n+m)/2$ even or odd is given in Fig. 12.

TABLE VII. Symmetries for pseudomorphic $(Si)_n/(Ge)_m$ SL's grown along the [001] direction.

$(Si)_n/(Ge)_m$	Space group	System	Lattice[a]
$n=m=1$	T_2^d	cubic	F
n,m even; $n+m=4k$	D_{2h}^5	orthorombic	P
n,m odd; $n+m=4k$	D_{2d}^5	tetragonal	P
n,m even; $n+m=4k+2$	D_{2h}^{28}	orthorombic	I
n,m odd; $n+m=4k+2$	D_{2d}^9	tetragonal	I
$n+m=$odd	D_{4h}^{19}	tetragonal	I

[a]F is face centered, P simple, and I body centered.

B. Electronic structure of $(Si)_n/(Ge)_n$ superlattices

As was previously done for the bulk materials, we use here a third-neighbor empirical tight-binding (TB) Hamiltonian with an sp^3 set of orbitals including spin-orbit interaction. As a consequence of the lattice deformation, there is a change in the distance between atoms and the bond angles. This will introduce some modifications, which are taken into account in the manner described in the preceding section. The strain dependence of the valence-band offset (VBO) has been also taken into account by interpolating between $\Delta E_v(\mathrm{Si})$, the VBO of strained Ge on Si(001), and $\Delta E_v(\mathrm{Ge})$, the VBO of strained Si on Ge(001).

$$\Delta E_v(x)=(1-x)\Delta E_v(\mathrm{Si})+x\Delta E_v(\mathrm{Ge}) \ , \tag{8}$$

where x is the concentration of Ge in the substrate, $\Delta E_v(\mathrm{Si})=0.84$ eV, and $\Delta E_v(\mathrm{Ge})=0.31$ eV.[65]

Figure 13 presents the band structure of a $(Si)_4/(Ge)_4$ SL grown on Si and Ge, as well as the strain-symmetrized one. For the case of a $(Si)_4/(Ge)_4$ SL grown on Si, because of the tetragonal distortion, the top valence state at Γ has p_x and p_y character, while the next lower one has p_z. They differ by 0.11 eV. For the same SL grown on Ge, the previous ordering of the states reverses and the energy difference becomes 0.15 eV. The conduction-band minima of the SL are along the $\Delta_{\parallel}$ ($\Delta_{\perp}$) directions for growth on the Si (Ge) substrate. Figure 14 presents the band structure of $(Si)_5/(Ge)_5$. For growth on the Ge(001)

substrate, the SL becomes a direct-gap material. The folding of the Brillouin zone produced by this superlattice periodicity brings the minimum of the Si conduction band to the Γ point. Indeed, theoretical calculations[16,18] predicted that this SL, grown on an appropriate substrate, becomes a direct-gap material.

In Fig. 15, the probability amplitude ($|\Psi|^2$) on the different atomic sites is shown for states at Γ of a $(Si)_4/(Ge)_4$ SL grown on Si and Ge. V_i (C_i) is the ith valence- (conduction-) band state at Γ, counting starts from the upper valence (lower conduction) state. In the same figure, the decomposition of the wave function in terms of the eigenstates of the average crystal[70] is presented. These results imply that valence states V_1 and V_2 are slightly confined in the Ge layers, while C_1 and C_2 are strongly confined in Si layers. This comes from the fact that the maximum of the Ge valence band is well above the corresponding maximum of Si, while the minimum of the conduction band of Si is below the corresponding minimum of Ge. In addition, the slight confinement of V_1 and V_2 in Ge has its origin in the small value of the effective mass of these hole states.

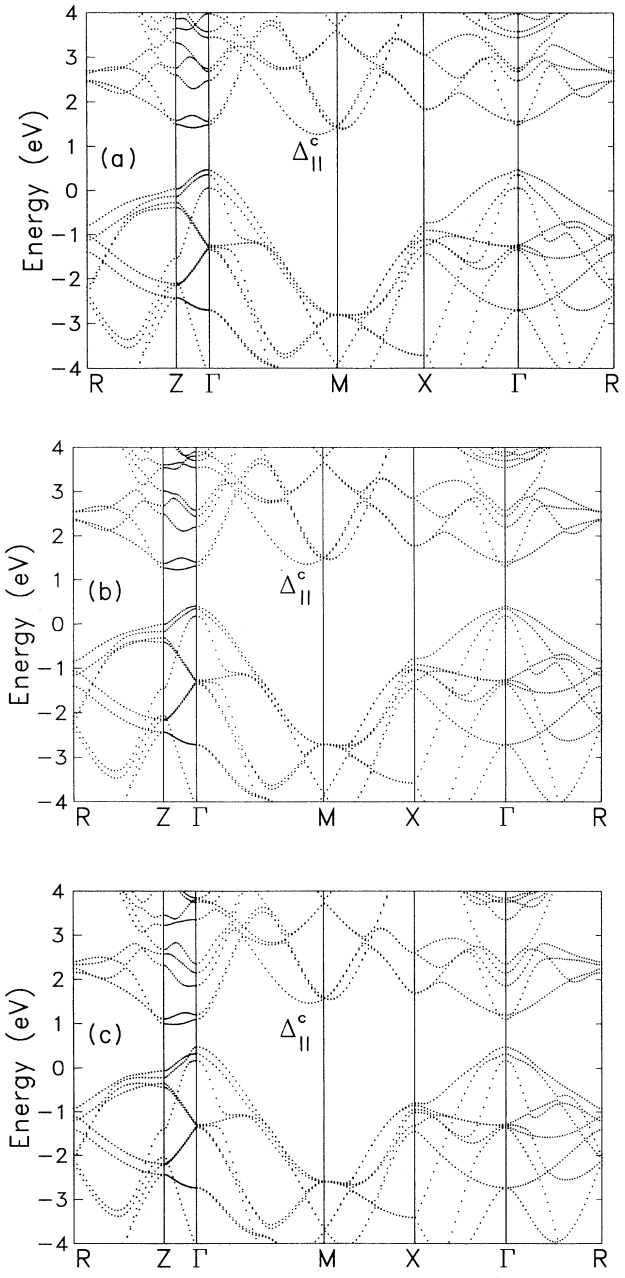

FIG. 13. The band structure of a $(Si)_4/(Ge)_4$ SL, (a) grown on Si(001), (b) strain symmetrized, and (c) grown on Ge(001).

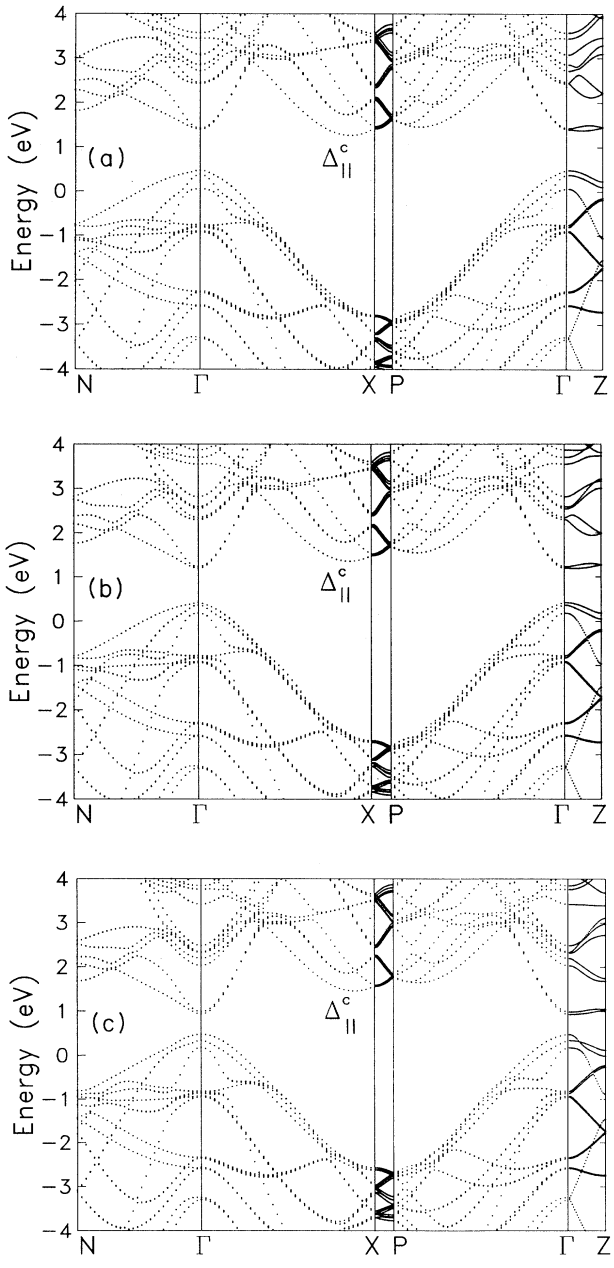

FIG. 14. The band structure of a $(Si)_5/(Ge)_5$ SL, (a) grown on Si(001), (b) strain symmetrized, and (c) grown on Ge(001).

State C_3 does not show confinement, C_4 is more or less confined at the interface, and finally C_5 is strongly confined in the Ge layers. Concerning the decomposition of the wave function, the conclusions are that V_1, V_2, and C_5 come mostly from Γ states, C_1 and C_2 from X states, and C_3 and C_4 mostly from Δ states of the average crystal. This is very important for the understanding of the transition probabilities between these states.

We have also calculated the transition probabilities between the valence V_i and conduction C_j states at Γ. In the calculation of $|M_{cv}(\mathbf{k})|^2$, where $M_{cv}(\mathbf{k})$ is the momentum matrix element between the valence and conduction states at $\mathbf{k}$, we have taken the mean value of this quantity for the three polarizations (x,y,z). The results are shown in Fig. 16. For the $(Si)_4/(Ge)_4$ SL, the states V_1 and V_2 as well as C_1 transform according to the Γ^+ representation of the double group, and C_2 according to Γ^-. As a result, the lowest permitted transitions are the V_1-C_2 and V_2-C_2. The probabilities for transitions V_1-C_2 and V_2-C_2 are two to three orders of magnitude lower than the transitions V_1-C_5 and V_2-C_5. This can be easily understood using the decomposition of the wave function in terms of the average crystal wave functions (Fig. 15). According to this analysis, V_1, V_2, and C_5 consist mostly of Γ states, and C_2 and C_2 mostly of X states of the average crystal. Thus the transition probabilities for V_1-C_2 and V_2-C_2 are considerably smaller than the V_1-C_5 and V_2-C_5 ones.

Regarding the transition probabilities for the case of the $(Si)_5/(Ge)_5$ SL, the results are similar to those of $(Si)_4/(Ge)_4$, the main difference being that in this case the V_1-C_1 transition is permitted. The value of the momentum matrix element is now up to three orders of magnitude smaller than the first transition, which has character of the average crystal (V_1-C_5). This property of the $(Si)_5/(Ge)_5$ SL, in conjunction with the existence of a direct gap, makes this superlattice a possible candidate for use in optoelectronic devices.

C. Influence of strain, superlattice periodicity, and composition

The lattice period and composition of a SL, as well as the strain produced by the substrate, influence the superlattice electronic properties. In Fig. 17, the variation, with respect to n, of the band gaps of the $(Si)_n/(Ge)_n$ SL is presented. The main conclusions drawn are the following.

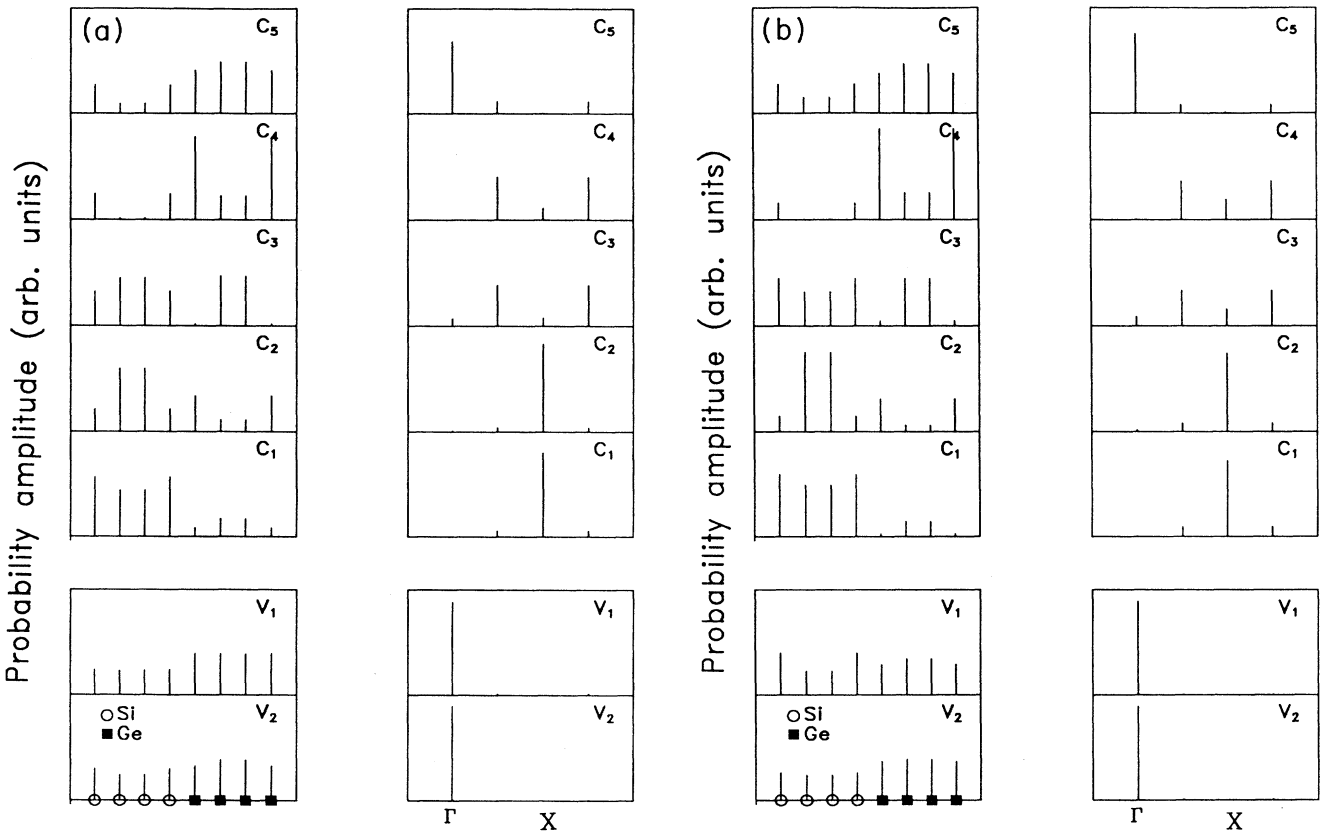

FIG. 15. The probability amplitude ($|\Psi|^2$) along different atomic sites for valence (V_i) and conduction (C_j) states at Γ for a $(Si)_4/(Ge)_4$ SL (left side). The decomposition of the corresponding wave function in terms of average crystal states (right side): (a) superlattice grown on Si(001) and (b) grown on Ge(001).

(a) For growth on Si, the fundamental gap is always indirect, it appears in the $\Delta_{\parallel}$ direction, and does not depend strongly on n. This is because the wave function of the corresponding conduction state extends in both materials. For the same SL, the direct gap has a totally different behavior. It depends strongly on n, and its value reduces for $n > 2$. This is due to the confined character of the lower conduction states at Γ.

(b) For strain-symmetrized SL's, as well as for growth on Ge, we get a totally different picture. Superlattices with $n = 5$ and 7 become direct-gap materials. The indirect gap for all cases appears in the $\Delta_{\perp}$ direction and its value depends on n, because this state is mostly confined in Si layers.

Figure 18(a) shows the dependence of the gaps on the composition x of the substrate alloy. The fundamental gap for the $(Si)_4/(Ge)_4$ SL is always indirect and in the direction $\Delta_{\parallel}$ ($\Delta_{\perp}$) for $x \lesssim 0.2$ ($x \gtrsim 0.2$). The similar behavior of direct and indirect gaps in the $\Delta_{\perp}$ direction comes from the fact that the corresponding conduction states have similar behavior, e.g., are confined in Si. The

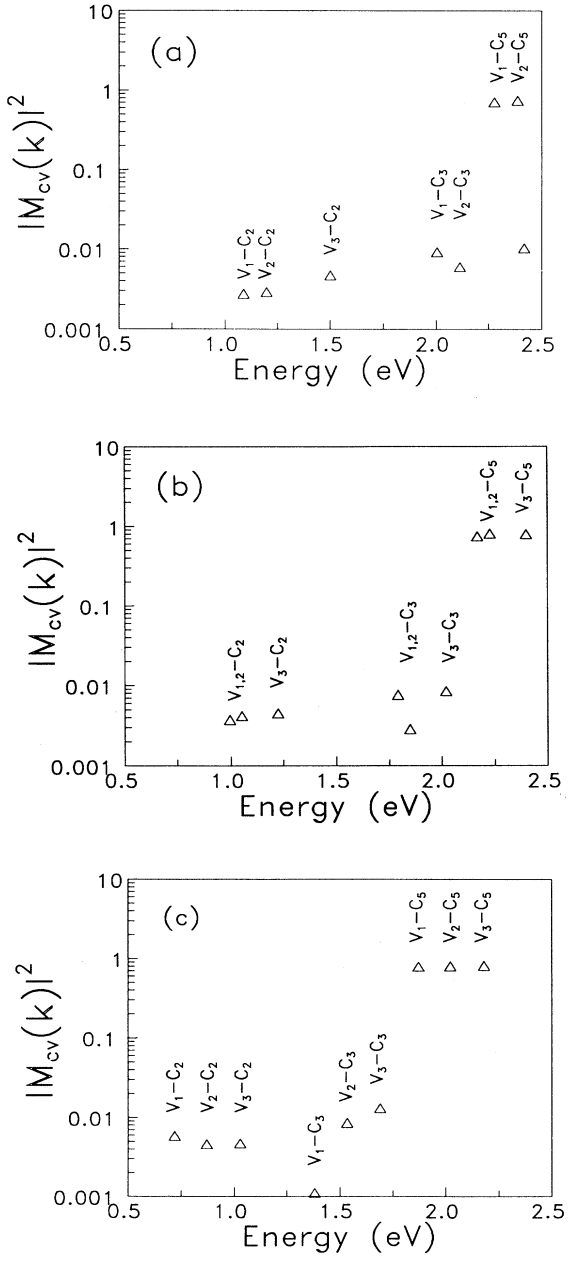

FIG. 16. Transition probabilities $|M_{cv}(\mathbf{k})|^2$ in units of $(h/a)^2$, between valence (V_i) and conduction (C_j) states at Γ, for superlattice $(Si)_4/(Se)_4$, (a) grown on Si(001), (b) strain symmetrized, and (c) grown on Ge(001).

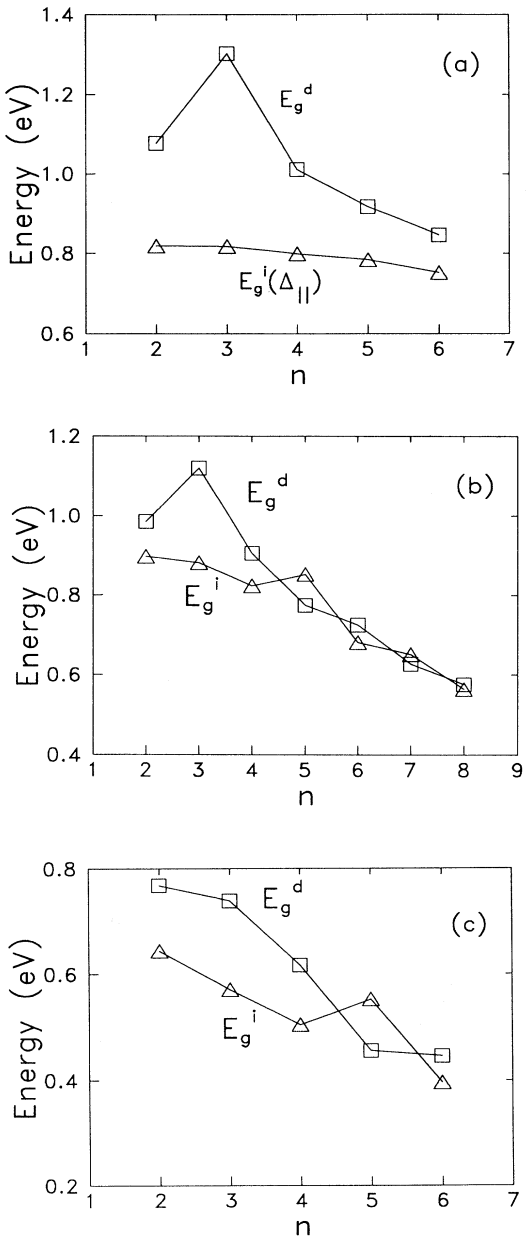

FIG. 17. Band gaps for different values of n for $(Si)_n/(Ge)_n$ SL's, (a) grown on Si(001), (b) strain symmetrized, and (c) grown on Ge(001).

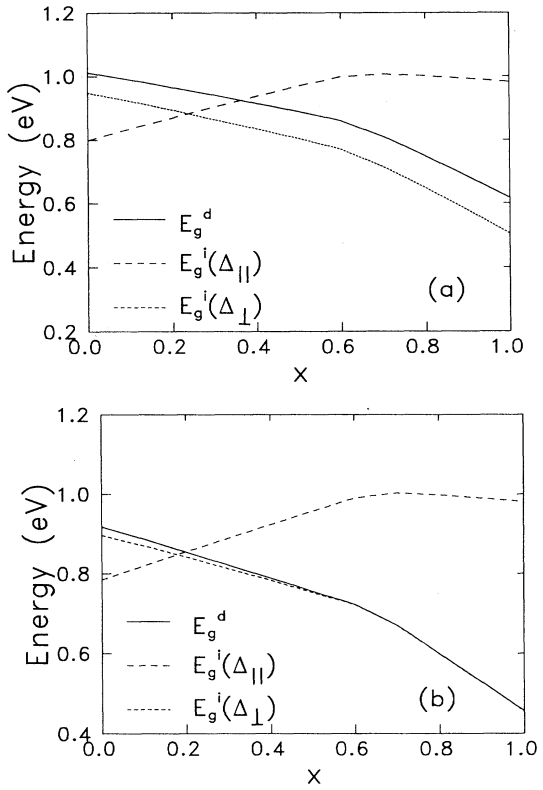

FIG. 18. Variation, as a function of x, of the direct (E_g^d) and indirect $\{E_g^i(\Delta_{\|})$ and $E_g^i(\Delta_{\perp})\}$ band gaps for SL's (a) $(Si)_4/(Ge)_4$ and (b) $(Si)_5/(Ge)_5$, grown on $Si_{1-x}Ge_x(001)$.

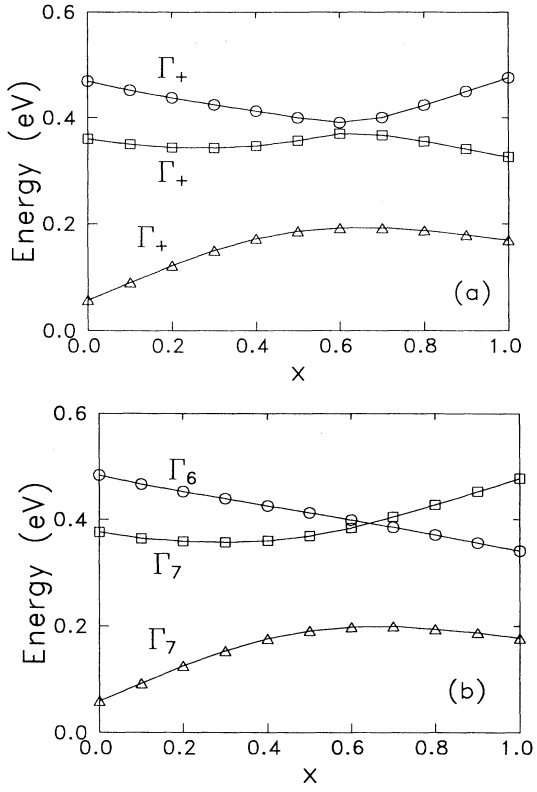

FIG. 19. Variation, as a function of x, of the energies at Γ of the three upper valence states of (a) $(Si)_4/(Ge)_4$ and (b) $(Si)_5/(Ge)_5$ SL's grown on $Si_{1-x}Ge_x(001)$.

slope change at $x \simeq 0.6$, in the variation of the gaps, is due to the anticrossing of the upper valence bands, as is shown in Fig. 19(a). For $x=0$, the upper valence band V_1 has heavy-hole, band V_2 light-hole, and band V_3 split-off characters. For $x=1$, the characters of V_1 and V_2 interchange, while that of V_3 remains the same.

The corresponding results for the $(Si)_5/(Ge)_5$ SL are presented in Figs. 18(b) and 19(b). In this case, the fundamental gap is indirect for $x \lesssim 0.6$ and in the direction $\Delta_{\|}$ ($\Delta_{\perp}$) for $x \lesssim 0.2$ ($0.2 \lesssim x \lesssim 0.6$). For $x \gtrsim 0.6$, no indirect gap in the $\Delta_{\perp}$ direction exists anymore, since it has collapsed to the Γ point. The behavior of valence states V_1, V_2, and V_3 for $(Si)_5/(Ge)_5$ is similar to that of $(Si)_4/(Ge)_4$, except that now states V_1 and V_2 cross at $x \simeq 0.6$.

Finally we have investigated the effect of the SL's composition on its electronic properties. For this purpose, we

TABLE VIII. Band gaps (in eV), transition energies (in eV), and the corrsponding transition probabilities (in units of h^2/a^2) of the lowest transition at Γ, for superlattices $(Si)_n/(Ge)_{10-n}$.

n	$E_g^d(\Gamma)$	$E_g^i(\Delta_{\|})$	$E_g^i(\Delta_{\perp})$	$\Delta E(V_i - C_j)$	$\lvert M_{cv}(\mathbf{k})\rvert^2$
			Si substrate		
3	0.980	0.730	0.956	$0.980(V_1-C_1)$	0.19×10^{-2}
4	0.902	0.751	0.897	$0.985(V_1-C_2)$	0.45×10^{-2}
5	0.917	0.784	0.897	$0.917(V_1-C_1)$	0.15×10^{-2}
6	0.918	0.815	0.897	$0.918(V_1-C_1)$	0.14×10^{-3}
7	0.959	0.868	0.930	$0.959(V_1-C_1)$	0.17×10^{-3}
			Ge substrate		
3	0.625	0.989	0.619	$0.625(V_1-C_1)$	0.29×10^{-2}
4	0.490	0.982		$0.590(V_1-C_2)$	0.76×10^{-2}
5	0.456	0.981		$0.456(V_1-C_1)$	0.31×10^{-2}
6	0.414	0.973		$0.593(V_2-C_1)$	0.36×10^{-3}
7	0.384	0.969		$0.434(V_1-C_2)$	0.23×10^{-2}

have studied superlattices of the form $(Si)_n/(Ge)_{10-n}$. These superlattices have the same folding of the BZ and similar band structure. Results for band gaps, the energy of the lowest allowed transition, as well as the corresponding transition probability are given in Table VIII. For growth on a Si(001) substrate, the fundamental gap is always indirect along the $\Delta_\parallel$ direction and increases with n. For growth on Ge, all superlattices with $n > 3$ have a direct gap, whose value decreases with n.

D. Effective masses

In order to study in detail the band behavior in the neighborhood of the center of the SBZ, we calculate the energy dispersion $E_n(\mathbf{k})$, using a fairly dense lattice of points, in the high-symmetry directions of the SBZ. In Fig. 20, the energy dispersion is shown in the vicinity of Γ for the three upper valence bands (V_1, V_2, V_3) and the two lower conduction bands (C_1, C_2), for the $(Si)_4/(Ge)_4$ SL grown on a Si(001) substrate, and for the [110], [1$\bar{1}$0], [100], and [001] directions. Note the anisotropy as well as the nonparabolic behavior of the valence bands in the (001) plane. This is due to the anticrossing of the bands close to the Γ point and the absence of spin degeneracy (Kramer's degeneracy) for SL's that do not exhibit inversion symmetry. On the other hand, parallel to the [001] direction the bands do not show the previously outlined behavior. We must, at this point, mention that all SL's studied in the present work exhibit similar dispersion of the bands near Γ. Figure 21 shows the energy dispersion close to Γ for a $(Si)_5/(Ge)_5$ SL grown on Si.

We calculate the effective masses for the holes, as well as the electrons for various directions, by fitting the energy bands very close to Γ with a fourth-order polynomial. Table IX shows the effective masses of the holes and the electrons for SL's $(Si)_n/(Ge)_n$ ($n=2-6$) grown on Si. The effective masses of the holes for the upper three valence bands have been calculated parallel to the [100] and [001] directions. From this table, we come to the conclusion that the change of the periodicity leaves almost unchanged the effective masses of the holes. This comes mainly from the fact that the superlattice potential

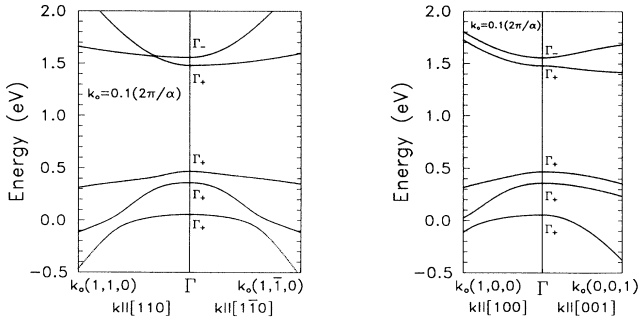

FIG. 20. The energy dispersion in the vicinity of Γ, and along the [110], [1$\bar{1}$0], [100], and [001] directions for the three upper valence and the two lower conduction bands, for a $(Si)_4/(Ge)_4$ SL grown on Si(001).

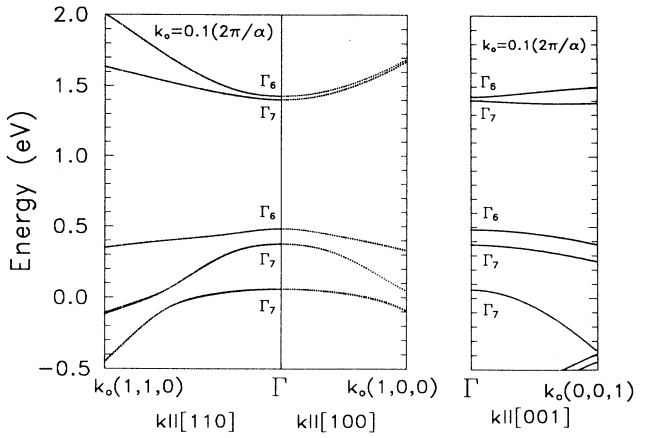

FIG. 21. The energy dispersion in the vicinity of Γ, and along the [110], [100], and [001] directions for the three upper valence and the two lower conduction bands, for a $(Si)_5/(Ge)_5$ SL grown on Si(001).

does not drastically influence the higher valence states at Γ, which are satisfactorily described by the corresponding average crystal states.[70]

Similar conclusion can also be drawn for the electron effective masses parallel to the growth plane. The effective masses at Γ for the [001] direction and the two lower conduction bands exhibit significant changes and strong dependence on the periodicity of the SL. We also note the appearance of a negative effective mass for band C_1, coming from the folding of the average crystal BZ. Also, the effective mass of the C_2 band for $(Si)_6/(Ge)_6$ on Si has a large value, which is due to the small dispersion of the corresponding band along the [001] direction. Another conclusion that can be drawn from Table IX is that parallel to the interface plane the effective mass of the higher valence state V_1 is smaller than that of V_2, while the opposite is true in the [001] direction. In Table IX, we also show the longitudinal ($m_e^\parallel$) and transverse ($m_e^\perp$) effective masses of the conduction-band extrema in the directions $\Delta_\parallel$ and $\Delta_\perp$. We remark that the electron effective masses at the extremum $\Delta_\parallel$ remain almost unchanged with n and take value close to the corresponding Si values. ($m_e^\parallel=0.568m_0, m_e^\perp=0.173m_0$). In the $\Delta_\perp$ direction, the former masses exhibit sizable variation. This comes from the confinement of the states along the growth axis. The mass $m_e^\perp(\Delta_\perp)$ does not change significantly, and takes values comparable to those of $m_e^\perp(\Delta_\parallel)$.

The dependence of the hole and electron masses on the composition of the SL is included in Table X, for SL's grown on a Si(001) substrate with $n+m=10$. States V_1 and V_2 are characterized by effective masses that change slightly with the variation of composition in the [100] direction. More precisely, they increase as the number of Si layers increases. Parallel to growth axis [001], the effective masses of bands V_1 and V_2 exhibit a more profound change, because they are influenced to a greater extent by the variation of the SL potential.

TABLE IX. Effective masses (in units of m_0) along the [100] and [001] directions for $(Si)_n/(Ge)_n$ SL's grown on Si(001).

	Holes					
$n:m$	$m_{V1}^{\parallel}$ [100]	$m_{V2}^{\parallel}$ [100]	$m_{V3}^{\parallel}$ [100]	$m_{V1}^{\perp}$ [001]	$m_{V2}^{\perp}$ [001]	$m_{V3}^{\perp}$ [001]
2:2	−0.156	−0.170	−0.487	−0.396	-0.370	−0.109
3:3	−0.155	−0.169	−0.452	−0.402	−0.335	−0.107
4:4	−0.156	−0.169	−0.444	−0.412	−0.327	−0.106
5:5	−0.157	−0.172	−0.444	−0.440	−0.339	−0.106
6:6	−0.163	−0.175	−0.448	−0.497	−0.366	−0.107

	Electrons							
$n:m$	$m_{C1}^{\parallel}$ [100]	$m_{C2}^{\parallel}$ [100]	$m_{C1}^{\perp}$ [001]	$m_{C2}^{\perp}$ [001]	$m_e^{\parallel}$ $\Delta_{\parallel}$	$m_e^{\perp}$ $\Delta_{\parallel}$	$m_e^{\parallel}$ $\Delta_{\perp}$	$m_e^{\perp}$ $\Delta_{\perp}$
2:2	0.213	0.215	−0.213	0.127	0.656	0.173	0.588	0.184
3:3	0.179	0.183	−0.040	0.038	0.621	0.171	0.636	0.186
4:4	0.197	0.195	−0.183	0.135	0.616	0.171	0.734	0.183
5:5	0.173	0.180	−0.258	0.188	0.622	0.172	0.950	0.180
6:6	0.185	0.184	−0.659	4.901	0.626	0.183		

The effective mass of the split-off band remains practically unchanged with respect to the composition of the SL. The electron effective masses of the $\Delta_{\parallel}$ extrema do not depend on the SL composition. In the [001] direction there is a different behavior. The composition influences the confinement of states in this direction and, as a result, there exists a considerable change of the effective mass $m_e^{\parallel}(\Delta_{\perp})$. The effective mass $m_e^{\perp}(\Delta_{\perp})$ practically does not change, and takes values close to those of Si.

Continuing our study, we have analyzed the dependence of the effective masses on the substrate, particularly for the $(Si)_4/(Ge)_4$ SL (orthorhombic symmetry) and $(Si)_5/(Ge)_5$ SL (tetragonal symmetry) cases, both grown on a $Si_{1-x}Ge_x(001)$ substrate with x ranging from 0 to 1. Figure 22 shows the dependence on x of the effective masses for the three upper valence bands of the $(Si)_4/(Ge)_4$ SL in the [110], [1$\bar{1}$0], [100], and [001] directions. The anisotropy in the effective masses for the V_3 state (s.o. character) parallel to the interfaces is almost negligible, while for the two upper valence states (with hh and lh character) parallel to the interface it is considerably stronger. In the [001] direction, the curves that describe the effective masses of bands V_1 and V_2 intercept close to $x=0.6$. This is a consequence of the anticrossing of V_1 and V_2 at that value of x. The effective masses close to $x=0.6$ for V_1 in the [110] direction, and V_2 in the [1$\bar{1}$0] direction, take large values. This comes from the fact that the corresponding bands become considerably flat for growth on a substrate with composition $x=0.6$. The variation of the effective mass in the [001] direction is shown in Fig. 22(d). In this case, the effective mass of V_3 increases with an increase of x, contrary to

TABLE X. Effective masses (in units of m_0) along the [100] and [001] directions for $(Si)_n/(Ge)_{10-n}$ SL's grown on Si(001).

	Holes					
$n:m$	$m_{V1}^{\parallel}$ [100]	$m_{V2}^{\parallel}$ [100]	$m_{V3}^{\parallel}$ [100]	$m_{V1}^{\perp}$ [001]	$m_{V2}^{\perp}$ [001]	$m_{V3}^{\perp}$ [001]
3:7	−0.138	−0.154	−0.442	−0.379	−0.314	−0.100
4:6	−0.148	−0.162	−0.443	−0.410	−0.325	−0.102
5:5	−0.157	−0.172	−0.444	−0.258	−0.440	−0.106
6:4	−0.168	−0.179	−0.445	−0.469	−0.349	−0.110
7:3	−0.172	−0.187	−0.442	−0.209	−0.352	−0.114

	Electrons							
$n:m$	$m_{C1}^{\parallel}$ [100]	$m_{C2}^{\parallel}$ [100]	$m_{C1}^{\perp}$ [001]	$m_{C2}^{\perp}$ [001]	$m_e^{\parallel}$ $\Delta_{\parallel}$	$m_e^{\perp}$ $\Delta_{\parallel}$	$m_e^{\parallel}$ $\Delta_{\perp}$	$m_e^{\perp}$ $\Delta_{\perp}$
3:7	0.189	0.183	−0.187	0.145	0.625	0.173	0.875	0.190
4:6	0.181	0.178	−0.392	0.450	0.620	0.174	1.484	0.183
5:5	0.173	0.180	−0.258	0.188	0.622	0.172	0.950	0.180
6:4	0.174	0.174	−0.319	0.213	0.611	0.173	0.862	0.178
7:3	0.170	0.171	−0.209	0.149	0.605	0.173	0.748	0.176

TABLE XI. Electron effective masses (in units of m_0) of a $(Si)_4/(Ge)_4$ SL grown on $Si_{1-x}Ge_x$, for different values of x.

x	$m_{C1}^{\parallel}$ [110]	$m_{C2}^{\parallel}$ [110]	$m_{C1}^{\perp}$ [001]	$m_{C2}^{\perp}$ [001]	$m_e^{\parallel}$ $\Delta_{\parallel}$	$m_e^{\perp}$ $\Delta_{\parallel}$	$m_e^{\parallel}$ $\Delta_{\perp}$	$m_e^{\perp}$ $\Delta_{\perp}$
0.0	0.113	0.760	−0.183	0.135	0.616	0.172	0.734	0.182
0.1	0.112	0.739	−0.182	0.138	0.613	0.174	0.743	0.180
0.2	0.112	0.717	−0.184	0.143	0.610	0.176	0.768	0.178
0.3	0.111	0.694	−0.187	0.148	0.607	0.178	0.794	0.176
0.4	0.110	0.669	−0.190	0.155	0.604	0.180	0.811	0.175
0.5	0.110	0.644	−0.193	0.162	0.602	0.182	0.841	0.172
0.6	0.109	0.617	−0.196	0.169	0.599	0.185	0.880	0.170
0.7	0.109	0.590	−0.198	0.177	0.597	0.187	0.897	0.169
0.8	0.108	0.563	−0.200	0.186	0.594	0.189	0.963	0.166
0.9	0.107	0.535	−0.202	0.195	0.592	0.191	0.979	0.164
1.0	0.107	0.508	−0.202	0.205	0.589	0.194	1.098	0.162

what happens parallel to the interface. The values of the electron effective masses are given in Table XI. Note the hole character exhibited by the state C_1 along the [001] direction, and that of the effective masses of C_1 and C_2 in the [110], [1$\bar{1}$0], and [001] directions, do not significantly depend on the substrate. Also, the effective masses $m_e^{\parallel}(\Delta_{\parallel})$, $m_e^{\perp}(\Delta_{\parallel})$, and $m_e^{\perp}(\Delta_{\perp})$ do not significantly depend on the substrate, while $m_e^{\parallel}(\Delta_{\perp})$ does. The reasons for this behavior have been stated in the previous analysis. In Fig. 23, the hole effective masses of the $(Si)_5/(Ge)_5$ SL parallel to the [100] and [001] directions are shown. In this case the effective masses parallel to the interfaces are isotropic. In Table XII, the dependence of the electron's effective masses on x is presented for the previous SL.

E. Spin splittings

It is well known that the spin-orbit interaction lifts the band states degeneracies, the most profound effect occur-

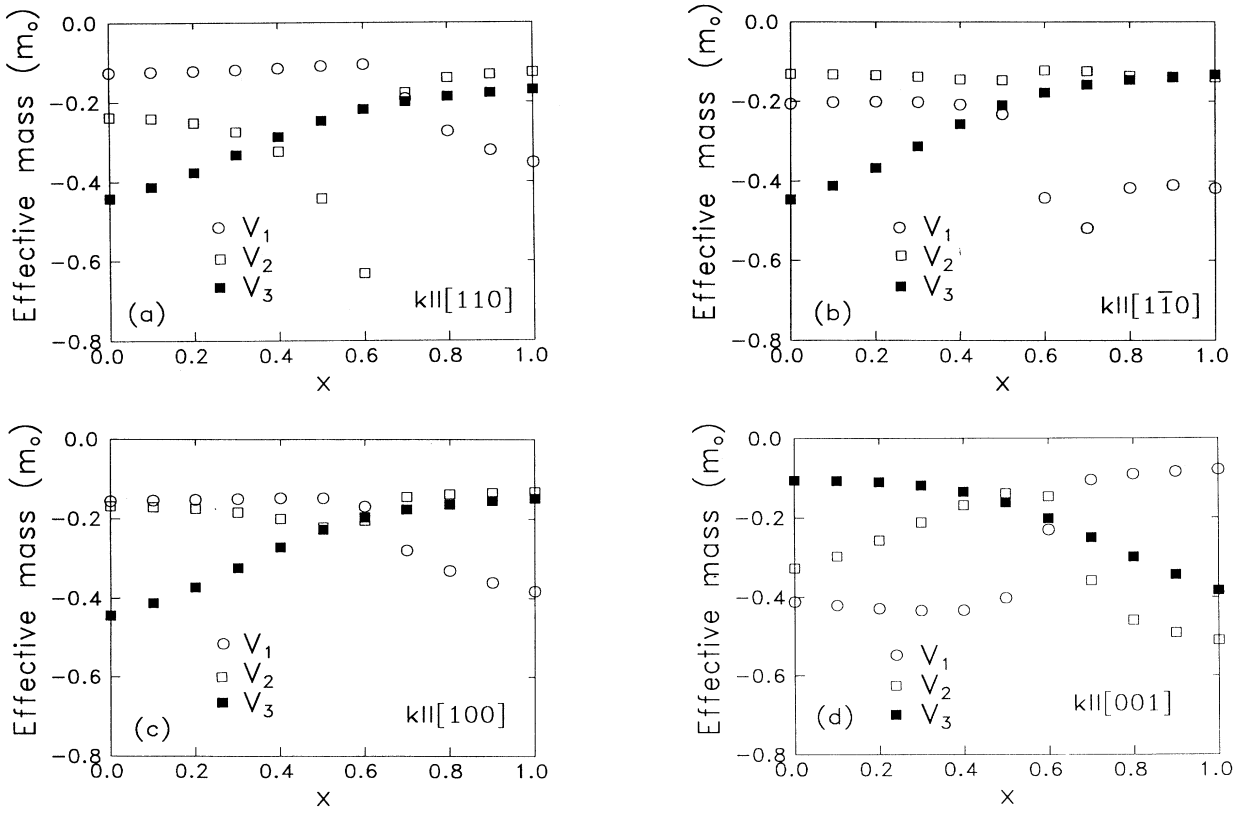

FIG. 22. Effective masses, in units of m_0, along the (a) [110], (b) [1$\bar{1}$0], (c) [100], and (d) [001] directions for the three upper valence states of a $(Si)_4/(Ge)_4$ SL, grown on $Si_{1-x}Ge_x(001)$, as a function of x.

TABLE XII. Electron effective masses (in units of m_0) of a $(Si)_5/(Ge)_5$ SL grown on $Si_{1-x}Ge_x$, for different values of x.

x	$m_{C1}^{\parallel}$ [100]	$m_{C2}^{\parallel}$ [100]	$m_{C1}^{\perp}$ [001]	$m_{C2}^{\perp}$ [001]	$m_e^{\perp}$ $\Delta_{\parallel}$	$m_e^{\perp}$ $\Delta_{\parallel}$	$m_e^{\parallel}$ $\Delta_{\perp}$	$m_e^{\perp}$ $\Delta_{\perp}$
0.0	0.173	0.180	−0.258	0.188	0.622	0.173	0.917	0.180
0.1	0.171	0.179	−0.332	0.222	0.617	0.175	0.942	0.179
0.2	0.169	0.177	−0.450	0.265	0.613	0.177	1.031	0.176
0.3	0.168	0.176	−0.640	0.317	0.610	0.179	1.085	0.174
0.4	0.166	0.175	−0.986	0.380	0.606	0.182	1.314	0.172
0.5	0.164	0.174	−1.785	0.454	0.603	0.184	1.765	0.169
0.6	0.162	0.173	−5.400	0.544	0.599	0.186	3.344	0.165
0.7	0.160	0.172	7.985	0.654	0.595	0.189	7.985	0.161
0.8	0.159	0.171	2.615	0.794	0.592	0.191	2.615	0.159
0.9	0.157	0.169	1.675	0.987	0.589	0.194	1.678	0.158
1.0	0.155	0.169	1.287	1.292	0.586	0.196	1.287	0.156

ring at high-symmetry points of the BZ. Also, when the crystal possesses inversion as well as time-reversal symmetry, then all the band states are at least twofold degenerate (Kramer's degeneracy). The lack of inversion symmetry has as a consequence the splitting, in general, of states with different spin orientation (this splitting will be called spin splitting). For instance, the $(Si)_n/(Ge)_m$ SL's with n and m odd do not possess inversion symmetry and therefore do not exhibit Kramer's degeneracy. Although this is true, there are some high-symmetry directions

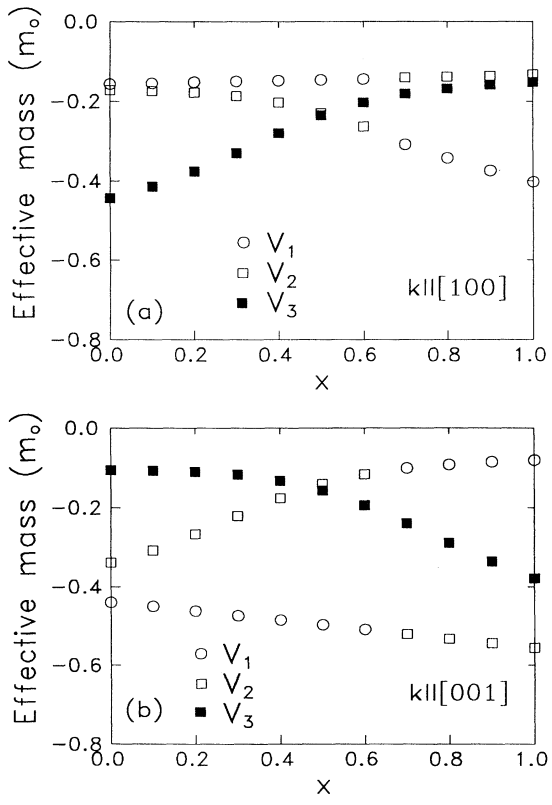

FIG. 23. Effective masses, in units of m_0, along the (a) [100] and (b) [001] directions for the three upper valence states of a $(Si)_5/(Ge)_5$ SL, grown on $Si_{1-x}Ge_x(001)$, as a function of x.

where band states are degenerate with respect to the spin quantum number. Also, it is known that strain produces a spin splitting that is linear in k,[71] e.g.,

$$|\Delta E| = Ck \ , \tag{9}$$

where k is the distance from the band extremum. The occurrence of such splittings near the band extrema can affect to a large degree the transport properties of the SL's.

In Fig. 24, the absolute values of the spin splittings are shown for the three upper valence and two lower conduction bands of the strain-symmetrized $(Si)_3/(Ge)_3$, $(Si)_5/(Ge)_5$, and $(Si)_7/(Ge)_7$ SL's. The larger spin splittings occur for **k** parallel to the interfaces, i.e., along the [100] direction, while they vanish in the perpendicular direction. The SL's with the thinner layers show larger splittings, compared to the thicker ones, because the lack of inversion symmetry is related to the interfaces. Fitting the spin splittings by a polynomial of third order, we find a nonzero linear term. The values of the coefficient C of the linear term, Eq. (9), are given in Table XIII. Its value for the upper valence state ($V1$) is quite a bit smaller compared to the corresponding ones for V_2 and V_3. Also, for the case of V_2 and V_3, it gets smaller as the periodicity increases.

F. Influence of VBO

As we have mentioned before, VBO is a significant parameter whose value influences the calculated band struc-

TABLE XIII. Coefficients of the linear term [Eq. (9)] for the spin splittings along the [100] direction of the three upper valence and the two lower conduction bands for the strain-symmetrized $(Si)_3/(Ge)_3$, $(Si)_5/(Ge)_5$, and $(Si)_7/(Ge)_7$ SL's.

	3:3	5:5	7:7
C_{V1}[a]	0.007	0.012	0.032
C_{V2}	0.218	0.131	0.073
C_{V3}	0.209	0.131	0.087
C_{C1}	0.008	0.024	0.041
C_{C2}	0.138	0.045	0.009

[a]The coefficients C are in units of $eV/(2\pi/a)$.

ture. The values for VBO almost exclusively used in recent calculations are those of Van de Walle and Martin.[65] Nevertheless, different values also appear in the bibliography.[72–74] In order to investigate the influence of VBO on the different band gaps, we have calculated the direct and indirect gaps of strain-symmetrized $(Si)_5/(Ge)_5$ and $(Si)_{10}/(Ge)_{10}$ SL's for values of VBO ranging from 0 to 1 eV (according to Ref. 65, the value of VBO in these SL's is 0.607 eV). The results of the calculation are presented in Fig. 25. According to these calculations, the $(Si)_5/(Ge)_5$ SL is a direct-gap material for all the values of VBO we have used. This gap, as well as the indirect gap at the Z point (E_g^Z), reduce their value as VBO increases. This is due to the fact that the Si/Ge SL's are of type II, with the top valence-band states slightly confined in the Ge layers and conductor states at Γ as well as in the ΓZ

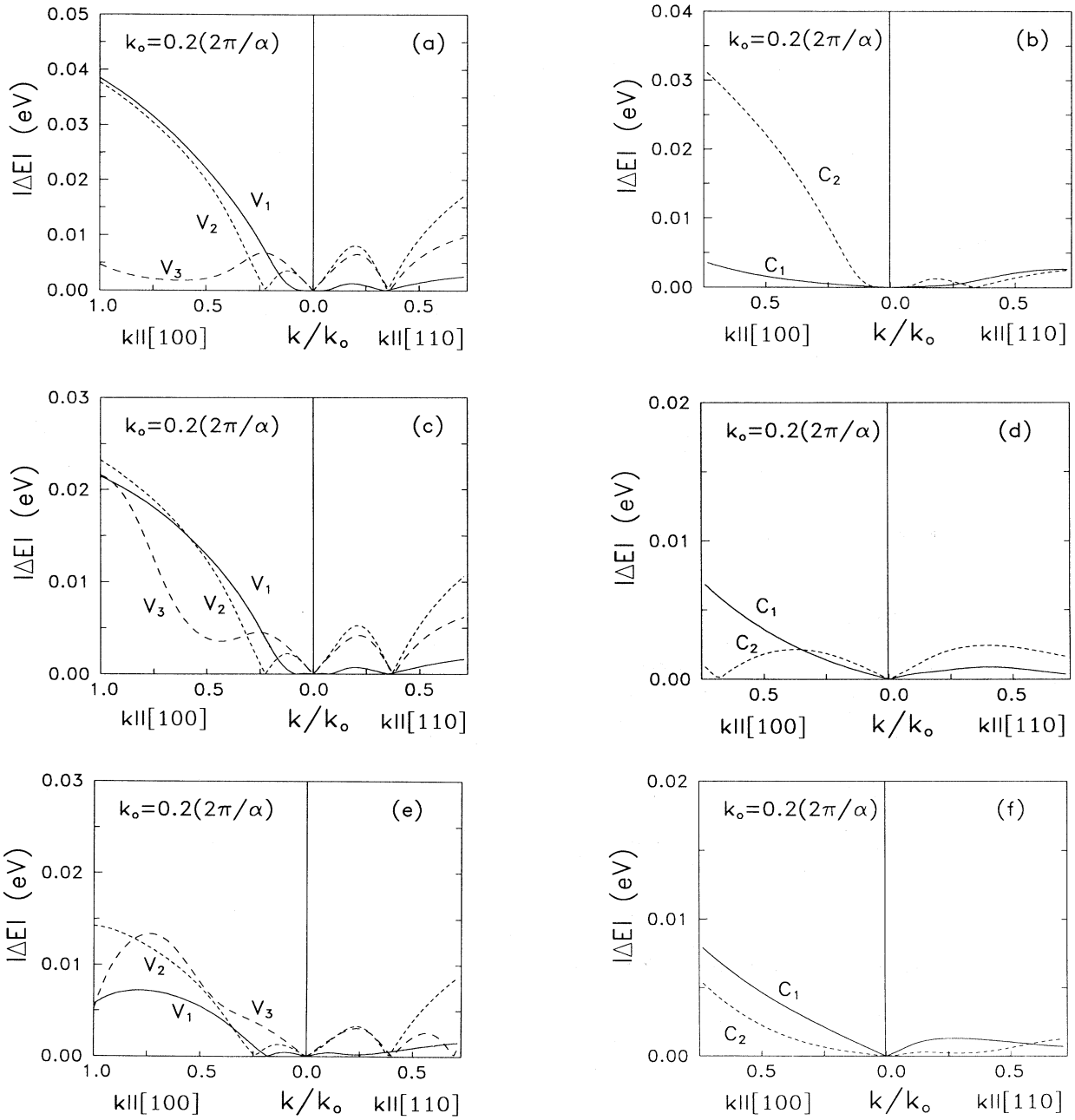

FIG. 24. Spin splittings as a function of k along the [100] and [110] directions, for the three upper valence (V_1, V_2, V_3) and the two lower conduction (C_1, C_2) bands for the strain-symmetrized $(Si)_3/(Ge)_3$ [(a) and (b)], $(Si)_5/(Ge)_5$ [(c) and (d)] and $(Si)_7/(Ge)_7$ [(e) and (f)] SL's.

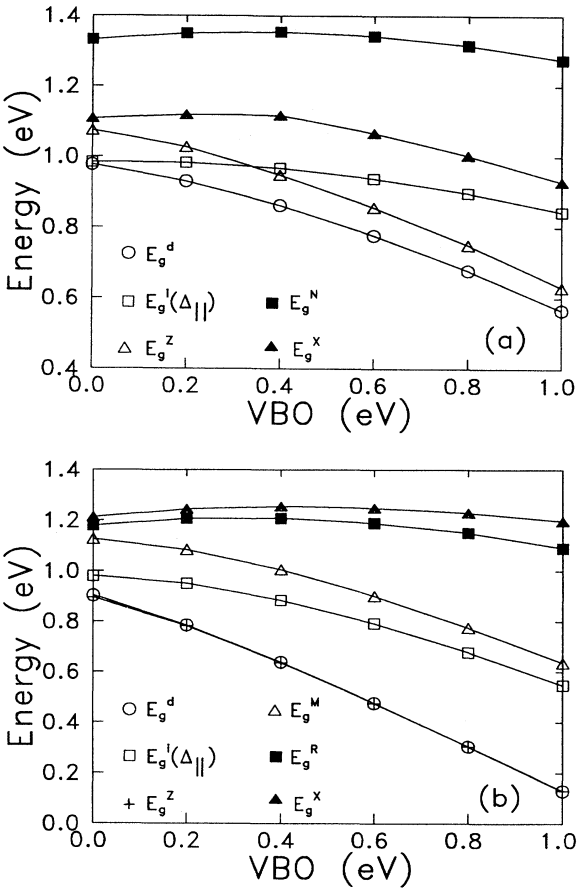

FIG. 25. The dependence of direct and indirect gaps on the VBO for strain-symmetrized (a) $(Si)_5/(Ge)_5$ and (b) $(Si)_{10}/(Ge)_{10}$ SL's.

direction confined in Si layers. As VBO increases, the top of the valence band approaches the bottom of the conduction band and, as a result, the band gap decreases. The indirect gaps $E_g^i(\Delta_\parallel)$ and E_g^X vary to a lesser degree and mostly for VBO larger than 0.4 eV. This is because the larger values of VBO produce stronger confinement in Si of conduction states at $\Delta_\parallel$ and X, resulting in a decrease of their energy. Gap E_g^N is practically independent of the value of VBO.

Superlattice $(Si)_{10}/(Ge)_{10}$ is almost a direct-gap material. The direct gap at Γ is almost degenerate with E_g^Z, since the lowest conduction band does not show dispersion in the ΓZ direction. VBO has now a stronger influence on gaps E_g^d and E_g^Z in comparison to the $(Si)_5/(Ge)_5$ SL. This is due to the fact that thicker SL's produce stronger confinement of the states.

We have also studied the influence of VBO on the transition probabilities at Γ. Our calculations show that the transition matrix elements remain almost invariant for the previously mentioned variation of VBO.

G. Comparison with experiment

It was stated in the Introduction that the experimental work on strained Si/Ge SL's mainly refers to electroreflectance and photoluminescence measurements. The first samples studied were finite SL's grown on Si or Ge. Then the interest turned to the study of strain-symmetrized SL's, since in this case larger crystals can be grown. On the other hand, the interpretation of the experimental results is a difficult task, because the SL's effects are small and many other contributions can have similar behavior. For example, in electroreflectance experiments, the Franz-Keldysh oscillations,[75] and optical etalon interference effects[76] can lead to spectra similar to the SL ones. In addition, some photoluminescence spectra may originate from defects. Also, special care should be exercised during growth to keep the periodicity constant throughout the sample. With this in mind we will try to compare theory and experiment, and find if there is some consensus between them with regard to the electronic structure of the SL's.

For the case of the strain-symmetrized $(Si)_6/(Ge)_4$ SL, Zachai *et al.*[9] reported strong photoluminescence close to 0.84 eV. They attributed this peak to a fundamental quasidirect band-gap transition with an enhanced dipole-allowed transition rate. Our calculations predict an almost direct-gap material with $E_g^i=0.797$ eV and $E_g^d=0.806$ eV. The first two direct transitions, with energies equal to 0.806 and 0.874 eV, are dipole allowed for polarization along the interfaces, with transition probabilities considerably smaller than the first Ge bulklike transition.

In very recent photoluminescence measurements on the strain-symmetrized $(Si)_5/(Ge)_5$ SL, Menczigar *et al.*[12] reported a peak at 0.76 eV, attributing it to a direct transition. Our calculations predict the existence of a direct transition at 0.77 eV, with appreciable transition probability, in excellent agreement with the experimental observation. Similar results have been given by Turton and Jaros,[16] using the empirical pseudopotential method.

We turn now to finite superlattices. In the case of a finite $(Si)_4/(Ge)_4$ SL on a Si(001) substrate, measurements were performed on a sample with a five-period superlattice embedded in Si. In electroreflectance spectra, the lower-energy structures were observed at 0.76, 1.03, and 1.23 eV. Our calculations, based on an infinite SL model, give that the lower transitions at Γ have energies of 1.09 and 1.20 eV, but with transition probabilities two to three orders of magnitude smaller than the E_0 bulklike transition. These energies differ significantly from the experimental value of 0.76 eV. On the other hand, the calculated indirect gap of this infinite SL is found equal to 0.80 eV, close to the value of 0.76 eV. Indeed, recent photocurrent[77] measurements attributed indirect character to the lowest transition found at 0.78 and 0.90 eV. In recent theoretical calculations for the finite crystal, we have found,[78] using the present model, that the lowest transitions with appreciable probabilities appear at 1.1 and 1.21 eV, close to the corresponding values for the infinite SL. Therefore, the results for the infinite and finite $(Si)_4/(Ge)_4$ SL's are not significantly different.

In the case of a $(Si)_4/(Ge)_6$ SL grown on a Ge(001) substrate, measurements have been performed by Pearsal *et al.*[6] on a sample with a five-period SL separated by a Ge spacer of about 200 Å thick. Transitions at 0.80,

0.96, 1.18, and 1.22 eV were found. The transitions at 0.88 and 1.18 eV were attributed to the E_0 and $E_0+\Delta_0$ structures of Ge, and the rest to SL transitions. Very recent piezoreflectance measurements by Yin *et al.*[10] on the same structure led to conclusions different from those of Ref. 6. They found that the observed structures (with the exception of those related to the substrate) result from transitions in the Ge spacer and not in the superlattice. For a Ge spacer of 78 monolayers, the lower transitions occur at 0.947 and 0.967 eV, while for 127 monolayers the former values become 0.915 and 0.926 eV, respectively. Recent theoretical calculations by the present authors,[78] using the present model, for the finite SL $[(Si)_4/(Ge)_6]_5/[Ge]_{48}$ support this interpretation. More precisely, the calculations predict the lower transitions with appreciable probabilities to occur at 0.99 and 1.01 eV and have been attributed to transitions in the Ge spacer.

All the previous analysis makes clear the usefulness of our model in the understanding of the electronic properties of superlattices.

IV. CONCLUSIONS

A new tight-binding model in the three-center representation, with an orthogonal sp^3 set of orbitals and interactions up to third neighbors, is introduced. This model reproduces known results for bulk Si and Ge, that is, their band structure, including the lowest conduction bands, density of states, effective masses, deformation potentials, and dielectric function. In addition, it is an efficient model as far as computer time is concerned; therefore it is most appropriate for application to systems with large unit cells, such as superlattices. As an application, the electronic structures of some $(Si)_n/(Ge)_m$ SL's have been studied. Their band structure, the confinement of the superlattice states and their decomposition in terms of the average crystal states, the effective masses, and the spin splittings, have been investigated as a function of their composition, strain, and layer thickness. For $(Si)_n/(Ge)_n$ SL's grown on a Ge(001) substrate we found that, for some cases, the gap changes from indirect to direct. In particular, $(Si)_5/(Ge)_5$ and $(Si)_7/(Ge)_7$ are direct-gap materials when grown on a Ge(001) substrate. The strain effects were studied for $(Si)_4/(Ge)_4$ and $(Si)_5/(Ge)_5$ SL's. The $(Si)_4/(Ge)_4$ SL is always an indirect-gap material while the $(Si)_5/(Ge)_5$ SL becomes a direct one when grown on a $Si_{1-x}Ge_x$ alloy buffer with $x>0.6$. By varying the concentration x of the buffer alloy, the top two valence-band states cross (anticross) at $x\simeq 0.6$ for the $(Si)_5/(Ge)_5$ $[(Si)_4/(Ge)_4]$ SL. Also, we found that $(Si)_n/(Ge)_{10-n}$ SL's are direct-gap materials when grown on a Ge (001) surface.

Valence bands were found to be anisotropic and nonparabolic for wave vectors parallel to the interfaces, but quite close to parabolic along the growth axis. In general, we found that the hole effective masses are unaffected by the strain, composition, and layer thickness, while the electron effective masses along the growth axis change a great deal. In addition, the spin splittings for $(Si)_3/(Ge)_3$, $(Si)_5/(Ge)_5$, and $(Si)_7/(Ge)_7$ SL's are appreciable (30–50 meV) parallel to the interfaces, but they vanish along the growth axis and become smaller for thicker SL's.

Finally, the comparison with experimental results shows that the present model is a realistic one and can be used to describe the electronic properties of the strained Si/Ge SL's and clarify many of the points which are under debate.

ACKNOWLEDGMENT

This work has been supported in part by the ESPRIT Basic Research Action No. 7128.

[1]E. Kasper, H. J. Herzog, H. Dambkes, and G. Abstreiter, in *Layered Structures and Epitaxy*, edited by J. M. Gibson, G. C. Osbourn, and R. M. Tromp, MRS Symposium Proceedings No. 56 (Materials Research Society, Pittsburgh, 1986).

[2]T. P. Pearsall, *Critical Reviews in Solid State and Materials Sciences* (CRC, Boca Raton, FL, 1989), Vol. 15, p. 551.

[3]S. C. Jain and W. Hayes, Semicond. Sci. Technol. **6**, 547 (1991).

[4]U. Gnutzman and K. Clausecker, Appl. Phys. **3**, 9 (1974).

[5]T. P. Pearsall, J. Bevk, L. C. Feldman, J. M. Bonar, J. P. Mannaerts, and A. Ourmazd, Phys. Rev. Lett. **58**, 729 (1987).

[6]T. P. Pearsall, J. M. Vandenberg, R. Hull, and J. M. Bonar, Phys. Rev. Lett. **63**, 2104 (1989).

[7]T. P. Pearsall, J. Bevk, J. C. Bean, J. Bonar, J. P. Mannaerts, and A. Ourmazd, Phys. Rev. B **39**, 3741 (1989).

[8]K. Asami, K. Miki, K. Sakamoto, T. Sakamoto, and S. Gonda, Jpn. J. Apl. Phys. **29**, L381 (1990).

[9]R. Zachai, K. Eberl, G. Abstreiter, E. Kasper, and H. Kibbel, Phys. Rev. Lett. **64**, 1055 (1990).

[10]Y. Yin, D. Yan, F. H. Pollak, M. S. Hybertsen, J. M. Vandenberg, and J. C. Bean, Phys. Rev. B **44**, 5955 (1991).

[11]J. Olajos, J. Engvall, H. G. Grimmeiss, H. Kibbel, E. Kasper, and H. Presting, in *International Conference on Electronic Materials, EMRS 1992 Spring meeting, Strasbourg-France* [Thin Solid Films (to be published)].

[12]U. Menczigar, J. Brunner, E. Friess, M. Gail, G. Abstreiter, H. Kibbel, H. Presting, and E. Kasper, *International Conference on Electronic Materials* (Ref. 11).

[13]U. Schmid, F. Lukes, N. E. Christensen, M. Alouani, M. Cardona, E. Kasper, H. Kibbel, and H. Presting, Phys. Rev. Lett. **65**, 1933 (1990).

[14]U. Schmid, J. Humlicek, F. Lukes, M. Cardona, H. Presting, H. Kibbel, E. Kasper, K. Eberl, W. Wegscheider, and G. Abstreiter, Phys. Rev. B **45**, 6793 (1992).

[15]E. Kasper, H. Kibbel, H. Jorke, H. Brugger, E. Friess, and G. Abstreiter, Phys. Rev. B **38**, 3599 (1988).

[16]R. J. Turton and M. Jaros, Mater. Sci. Eng. B **7**, 37 (1990).

[17]S. Satpathy, R. M. Martin, and C. G. Van de Walle, Phys. Rev. B **38**, 13 237 (1988).

[18]U. Schmid, N. E. Christensen, M. Alouani, and M. Cardona, Phys. Rev. B **43**, 14 597 (1991).

[19]M. S. Hybertsen and M. Schluter, Phys. Rev. B **36**, 9683 (1987).

[20]P. Friedel, M. S. Hybertsen, and M. Schluter, Phys. Rev. B **39**, 7974 (1989).
[21]S. Froyen, D. M. Wood, and A. Zunger, Phys. Rev. B **36**, 4547 (1987); **37**, 6893 (1988).
[22]S. Ciraci and P. I. Batra, Phys. Rev. B **38**, 1835 (1988).
[23]I Morrison, M. Jaros, and K. B. Wong, Phys. Rev. B **35**, 9693 (1987).
[24]K. B. Wong, M. Jaros, I. Morrison, and J. P. Hagon, Phys. Rev. Lett. **60**, 2221 (1988).
[25]H. Rucker, R. Enderlein, and F. Bechstedt, Phys. Status Solidi B **153**, 595 (1989).
[26]L. Brey and C. Tejedor, Phys. Rev. Lett. **59**, 1022 (1987).
[27]M. A. Gell, Phys. Rev. B **38**, 7535 (1988); **40**, 1966 (1989).
[28]C. Tserbak, H. M. Polatoglou, and G. Theodorou, Europhys. Lett. **18**, 451 (1992).
[29]E. Ghahramani and J. E. Sipe, Phys. Rev. B **40**, 1102 (1989).
[30]E. Ghahramani, D. J. Moss, and J. E. Sipe, Phys. Rev. B **41**, 5112 (1990); **42**, 9193(E) (1990).
[31]W. A. Harisson, *Electronic Structure and Properties of Solids* (Freeman, San Francisco, 1980).
[32]K. C. Pandey and J. C. Phillips, Phys. Rev. B **13**, 750 (1976).
[33]L. F. Mattheiss and J. R. Patel, Phys. Rev. B **23**, 5384 (1981).
[34]P. Vogl, H. P. Hjalmarson, and D. Dow, J. Phys. Chem. Solids **44**, 365 (1983).
[35]D. A. Papaconstantopoulos, *Handbook of the Band Structure of Elemental Solids* (Plenum, New York, 1986).
[36]S. Y. Ren and W. A. Harrison, Phys. Rev. B **23**, 762 (1981).
[37]D. J. Moss, E. Chahramani, J. E. Sipe, and H. M. Van Driel, Phys. Rev. B **34**, 8758 (1986).
[38]J. R. Chelikowsky and M. L. Cohen, Phys. Rev. B **14**, 556 (1976).
[39]R. R. L. Zucca and Y. R. Shen, Phys. Rev. B **1**, 2668 (1970).
[40]G. E. Jellison and F. A. Modine, Phys. Rev. B **27**, 7466 (1989).
[41]S. Zwerdling, B. Lax, L. M. Roth, and K. J. Button, Phys. Rev. **114**, 80 (1959).
[42]L. Ley, S. P. Kowalczyk, R. A. Pollak, and D. A. Shirley, Phys. Rev. Lett. **29**, 1088 (1972).
[43]W. D. Grobman and D. E. Eastman, Phys. Rev. Lett. **29**, 1508 (1972).
[44]H. D. Barber, Solid-State Electron. **10**, 1039 (1987).
[45]R. N. Dexter, H. J. Zeiger, and B. Lax, Phys. Rev. **104**, 637 (1956).
[46]R. L. Aggarwal, Phys. Rev. B **2**, 446 (1970).
[47]J. C. Hensel, H. Hasegawa, and M. Wakayama, Phys. Rev. **138**, A225 (1965).
[48]D. Fink and R. Braunstein, Phys. Status Solidi B **73**, 361 (1976).
[49]G. Beni and T. M. Rice, Phys. Rev. B **9**, 4219 (1977).
[50]Y. Petroff, M. Balkanski, J. P. Walter, and M. L. Cohen, Solid State Commun. **7**, 459 (1968).
[51]P. Lautenschlager, M. Garriga, L. Vina, and M. Cardona, Phys. Rev. B **36**, 4821 (1987).
[52]C. Kittel, *Introduction to Solid State Physics* (Wiley, New York, 1976).
[53]L. Vina, S. Logothetidis, and M. Cardona, Phys. Rev. B **30**, 1979 (1984).
[54]J. C. Slater and K. F. Koster, Phys. Rev. **94** 1498 (1954).
[55]L. Brey, C. Tejedor, and J. A. Verges, Phys. Rev. B **29**, 6340 (1984).
[56]J. A. Verges, D. Glotzel, M. Cardona, and O. K. Anderson, Phys. Status Solidi B **113**, 519 (1982).
[57]C. Priester, G. Allan, and M. Lannoo, Phys. Rev. B **37**, 8519 (1988).
[58]F. H. Pollak and M. Cardona, Phys. Rev. **172**, 816 (1968).
[59]Author, in *Zahlenwerte und Funktionen aus Naturwissenschaften und Technik,* edited by K. H. Hellwege, Landolt-Börnstein, New Series, Group III, Vol. 17a (Springer-Verlag, Berlin, 1982).
[60]L. D. Laude and F. H. Pollak, Phys. Rev. B **3**, 2623 (1971).
[61]A. R. Goni, K. Syassen, and M. Cardona, Phys. Rev. B **39**, 12 921 (1989).
[62]I. Balslev, Phys. Rev. **143**, 636 (1966).
[63]W. Paul and D. M. Warschauer, in *Solids under Pressure,* edited by W. Paul and D. M. Warschauer (McGraw-Hill, New York, 1963).
[64]M. Chandrasekhar and F. H. Pollak, Phys. Rev. B **15**, 2127 (1977).
[65]C. G. Van de Walle and R. Martin, Phys. Rev. B **34**, 5621 (1986).
[66]J. Zi, K. Zhang, and X. Xie, Appl. Phys. Lett. **57**, 165 (1990).
[67]S. Ciraci, A. Baratoff, and I. P. Batra, Phys. Rev. B **41**, 6069 (1990).
[68]M. I. Alonso, M. Cardona, and G. Kanellis, Solid State Commun. **69**, 479 (1989); **70**, i (1989).
[69]P. Molinas i Mata, M. I. Alonso, and M. Cardona, Solid State Commun. **74**, 347 (1990).
[70]C. Tserbak, H. M. Polatoglou, and G. Theodorou, Phys. Rev. B **45**, 4327 (1992).
[71]O. E. Kane, in *Semiconductors and Semimetals,* edited by R. K. Willardson and A. C. Beer (Academic, New York, 1966), Vol. 1.
[72]W. A. Harrison and J. J. Tersoff, J. Vac. Sci. Technol. B **4**, 1068 (1986).
[73]L. Colombo, R. Resta, and S. Baroni, Phys. Rev. B **44**, 5572 (1991).
[74]T. F. Kuech, M. Maenpnaa, and S. S. Lau, Appl. Phys. Lett. **39**, 245 (1981).
[75]Y. Yin, D. Yan, F. H. Pollak, G. D. Pettit, and J. M. Woodall, Phys. Rev. B **43**, 12 138 (1991).
[76]A. C. Churchill, P. C. Klipstein, C. J. Gibbings, M. A. Gell, M. E. Jones, and C. G. Tuppen, Semicond. Sci. Technol. **6**, 18 (1990).
[77]M. S. Hybertsen, M. Schluter, R. People, S. A. Jackson, D. V. Lang, T. P. Pearsall, J. C. Bean, J. M. Vandenberg, and J. Bevk, Phys. Rev. B **37**, 10 195 (1988).
[78]H. M. Polatoglou, C. Tserbak, and G. Theodorou, in *Internationl Conference on Electronic Materials* (Ref. 11).